Do Heavy Ions Induce the Bystander Effect?
Study to determine the induction of the bystander effect from Fe ion beam compared to x-rays in human keratinocytes

by
Vered Anzenberg

Submitted to the Department of Nuclear Engineering in partial fulfillment of
the requirements for the degree of

Master of Science in Nuclear Engineering
at the
MASSACHUSETTS INSTITUTE OF TECHNOLOGY

[September 2005]
August 2005
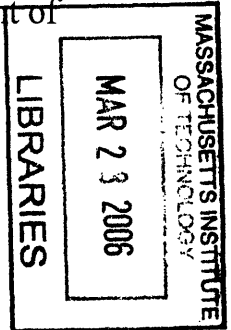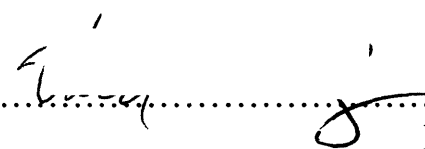
Author...
Department of Nuclear Engineering
August 8, 2005

Certified by...
Kathryn D. Held
Associate Professor, Harvard Medical School
Associate Radiation Biologist, Massachusetts General Hospital
Thesis Supervisor

Read by...
Jacquelyn C. Yanch
Professor of Nuclear Engineering, MIT
Thesis Reader

Accepted by...
Jeffrey Coderre
Chairman, Departmental Committee on Graduate Students

Do Heavy Ions Induce the Bystander Effect?

Study to determine the induction of the bystander effect from Fe ion beam compared to x-rays in human keratinocytes

by

Vered Anzenberg

Submitted to the Department of Nuclear Engineering on August 8, 2005 in partial fulfillment of the requirements for the degree of Master of Science in Nuclear Engineering

Abstract

The bystander effect is the observation that non-irradiated cells near a cell traversed by radiation express biological responses such as micronuclei formation and genomic instability. Most published studies of the bystander effect have been conducted using alpha particles, a high LET radiation. A few studies have been done with low LET radiation. This project studies the bystander effect from both low LET x-rays and high LET Fe particle beam irradiation. Using a transwell insert system, the bystander effect was studied in hTERT immortalized human keratinocytes. Cells are plated in a 6-well plate and in a companion permeable membrane insert. Cells in the 6-well plate are irradiated using conventional 250 kVp X-rays or 1000 MeV/nucleon Fe ion beam, LET of 151 keV/μm, from the NASA Space Radiation Laboratory at Brookhaven National Lab. After irradiation, inserts are immediately placed into the 6 well plate so that the irradiated and unirradiated cells are sharing medium but are not in contact. For both beams, frequency of micronuclei, chromatin bridges, and $p21^{Wafl}$ induction as well as cell cycle phase analysis were determined in both directly irradiated and bystander cells from 0.1 Gy to 5 Gy. From x-rays, a two-fold bystander effect at 24 h after irradiation with elevated $p21^{wafl}$ induction and micronuclei was seen but in Fe ion irradiation, the $p21^{wafl}$ bystander effect was delayed to 40-50 h after irradiation and no MN bystander effect was observed. Cell cycle analysis showed a slight G2 arrest in keratinocytes 5 h after x-rays but a strong G2 arrest until 40-50 h was seen after Fe ion irradiation. Bystander keratinocytes co-cultured with directly irradiated human fibroblasts AGO1522 cells showed a two-fold $p21^{wafl}$ and MN bystander effect 24 h after x-rays, and a potential 2-fold MN bystander effect 50 h after Fe ions. Bystander AGO1522 cells co-cultured with directly irradiated keratinocytes showed a two-fold MN bystander effect 24 h after x-rays, but no MN bystander response was seen at any time points studied from Fe ions. Striking differences in the bystander response were shown from the two radiation types, but the reason remains to be clarified.

Thesis Supervisor: Kathryn D. Held
Title: Associate Professor, Harvard Medical School
Associate Radiation Biologist, Massachusetts General Hospital

Acknowledgments

I wish to give thanks to my co-workers at Massachusetts General Hospital for both the stimulating biology discussions and the non-biological ones as well. Thank you to the support staff and scientists at Brookhaven National Laboratory, NASA Space Radiation Laboratory. Special thanks to Kamini Mahase for not only helping me with my experiments but also for being a great friend.

Special thanks to Dr. Hongying Yang for her advice on experiments, great thought provoking discussions, constant support in my work and future endeavors and for the great comments on my master's thesis.

I would like to thank all the great mentors that I have had in the past years both at UC Berkeley and at MIT. Special thanks to Dr. Jacquelyn Yanch for being both a great advisor and a strong supporter of my work. Deepest gratitude to Dr. Kathy Held for being an encouraging mentor and dedicated advisor. It has been a great honor to work in your lab.

I would like to thank all my friends, both in the states and abroad, for the support and friendship that I have been most blessed to have over the years. Most of all, I would like to thank my always-supporting family: my Dad, Mom, Alex, Eitan, and Paula. You have always allowed me to follow my dreams, and for that I am forever grateful.

Contents

Bibliography

List of Figures

List of Tables

Chapter 1

Introduction

Radiation dosimetry is the branch of nuclear science that quantifies the changes in a chemical and/or biological target due to radiation. When radiation interacts with a human cell, it deposits energy within the cell, which produces excited and ionized atoms. The linear energy transfer, LET, characterizes the amount of energy that is deposited within the cell per unit distance along the charged particle track. This energy can create chemically active species or directly damage the DNA helix, which ultimately can either cause cell death, or if the DNA is inappropriately repaired, a possibility of neoplastic transformation, which may lead to cancer. Therefore, it is important to characterize the exposure of radiation, or the dose, that an individual is receiving in order to assess the possible biological damage.

The estimates used for cell damage are currently based on the theory that a cell is damaged only if radiation traversed the cell. However, in the past decade, there has been evidence by several independent research groups that indicates higher damage within cell cultures than expected based on the number of cells traversed by the radiation, and the term bystander effect has been coined to describe the response (Nagasawa and Little 1999; Mothersill and Seymour 2001; Yang et al. 2005). The bystander effect is the observation that non-irradiated cells near a cell traversed by radiation express biological

responses such as micronuclei formation (MN), genomic instability and cell cycle related gene expression induction (Azzam et al. 1998; Nagasawa and Little 1999). Several research groups have concluded that some signal is being transferred from the irradiated cells to the non-irradiated cells, which is also causing DNA damage in the non-irradiated cells.

Astronauts during space flight are exposed to radiation backgrounds composed of trapped proton and electron radiation, galactic cosmic rays made up of energetic protons and heavy ions, and sun radiation. The high LET components of the galactic cosmic rays, the heavy ions and energetic protons compose approximately 10-30% of the dose on a shuttle mission (Wilson 2000). Current carcinogenesis risks for low LET radiation are determined by linear back extrapolation from data at high doses of low LET radiation (x-rays and gamma rays). Carcinogenesis risks for high LET radiation are determined by making assumptions of greater biological damage than from low LET radiation. Previous experimental results have shown an increase in cell death due to the bystander effect from low LET radiation and alpha particles, but there has been little study of the bystander effect with heavy ion radiation as found in space. National Aeronautics and Space Administration, NASA, is specifically concerned with the possible increase in biological effects from exposure to space radiation environments and the biological effects from energetic protons and high LET radiation on the molecular level. Therefore, it is important to study the bystander effect for a broader range of radiation qualities, more specifically for heavy ions and highly energetic protons as encountered by astronauts, and compare it to the bystander effect seen with low LET radiation. The goal of this project is to study the induction of the bystander effect by heavy ions, such as Fe ions, and compare

the bystander results to those obtained with conventional x-rays. This project seeks to develop and answer three aims:

1. Determine the occurrence of bystander effect(s) from conventional x-rays in a cultured keratinocyte cell line. Dose response curves will be obtained for the induction of the bystander effect.

2. Determine the occurrence of bystander effect(s) from Fe ions at the NASA Space Radiation Lab at Brookhaven National Laboratory. Dose response curves will be obtained for the induction of the bystander effect for the same biological endpoints as for the conventional x-rays. Compare results from Fe ions to those of x-rays. (Low and high LET comparison)

3. Determine the induction of the bystander effect(s) from Fe ions and conventional x-rays from human fibroblasts co-cultured with keratinocytes and vice versa.

1.1 Space Radiation Environment

NASA's current plan for future missions includes a potential manned mission to Mars, long-term missions to the lunar surface, and the International Space Station (ISS). Earth's magnetic field shields equipment and people from a large portion of the radiation in earth's orbit but outside the earth's field, the radiation environment is drastically different. Two keys points must then be considered: shielding astronauts from the radiation environment, and determining biological effects from the types of radiation in space.

Earth's atmosphere is an equivalent of 10 m of water and shields cosmic ray levels on earth to give an annual background dose of 0.27 mSv, which is only 8% of our annual background dose of 3 mSv (Turner 1995; Wilson 2000). An astronaut who will

reside on the ISS for 4-6 months is estimated to receive an approximate dose of between 8-20 cSv, a 30 fold increase over annual background dose rates on earth (Cucinotta 2000). More importantly, an astronaut is going to receive more fractioned and higher dose rates of exposure 24 h each day, unlike any other occupational exposures (Cucinotta 2000; Wilson 2000). In addition, occupational limits to NASA astronauts are higher than any other terrestrial radiation workers. When looking at risk assessment for space travel, the types of radiation must be considered.

1.1.1 Types of Radiation in Space

There are three main types of radiation in space: galactic cosmic rays (GCR), earth's radiation belts (van Allen radiation belts), and solar particle events. The energies and types of the particles will vary greatly due to the shielding from the spacecraft. However, the radiation environment will be due to both the primary particles as well as any secondary particles that could be formed.

Galactic cosmic rays are largely highly energetic protons and heavier ions, with a 2% component of electrons and positrons. Abundances of heavy ions decrease as atomic number increases, but peak again at iron. GCR are emitted isotropically in space, have roughly constant fluence, and have a broad energy spectrum, peaking at about 1 GeV/nucleon. The source of GCR is unknown, but outside our solar system. Solar events can change and influence the GCR fluence. It is estimated that 10-30% of whole body dose on shuttle missions is due to GCR (Wilson 2000).

The second type of radiation in space is from charged particles trapped in the van Allen radiation belts in a magnetic field surrounding the earth. The inner belt is mostly protons with energies above 10 MeV. The outer belt is mostly electrons of energies above

10 MeV. These belts are a problem for space travel when a spaceship passes through them and can be an issue for both the electronics and for the astronauts.

The third type of radiation occurs from solar particle events (SPEs) from the sun. The sun produces a constant flux of predominately low energy protons. However when a magnetic storm occurs on the sun, this can cause solar flares of increased radiation. Strong space weather with lethal doses occurring over very short periods of time has also been recorded. The majority of SPEs are high-energy protons and can create a noteworthy radiation risk to astronauts. Monitoring for SPEs occurs on the spacecraft, and "storm shelters" have been built for protection for the astronauts. A round trip to Mars is projected to take 3 years. An SPE event is probably likely within that time period. More importantly the risk from SPEs comes when an astronaut is out of the shuttle or on the lunar or Martian surface.

1.1.2 Risk from Space Radiation

Risk estimation based on experimental measurement for the radiation in space is nearly non-existent. Some high-energy protons are known to have a biological effectiveness value close to 1. Even though only about 10-30% of the space radiation fluence is the high-energy high Z particles (HZE), these represent the greatest risk. The quality factor associated for missions dominated with GCR radiation is currently set at 2.5 (Cucinotta 2000; Wilson 2000). However, the main concern for NASA is due to the long-term missions such as on ISS or Mars where the current projections of risk models for late effects from heavy ions and neutrons are not so dependable (Cucinotta 2000).

Space radiation is predominately low fluences of high LET radiation with rates at maximum (with no solar event activity) of: 4 protons /cm^2 sec, 0.4 helium ions/ cm^2 sec

and 0.04 HZE particles/ cm^2 sec with energies of a few hundred MeV to several GeV/ nucleon (Curtis and Letaw 1989). For a typical cell nucleus of 100 μm^2, each cell nucleus in the body would receive a proton every 3 days, helium once a month, and a HZE particle (high atomic number and energy) once per year (Curtis and Letaw 1989). With such low fluences, the real risk is from late effects from space travel. Current risk assessment is done with knowledge of high doses, from 0.5 –2 Gy, that were delivered as one single shot at high dose rates of low LET radiation. Risk in the low dose region is then determined by linear back extrapolation to low doses and assumptions are made to correct for low dose rates and for high LET (BEIRVII 2005). At doses below 1 Gy, risk estimation offers three models: linear no threshold, threshold and linear quadratic. The choice of model will affect greatly the radiation protection and associated risk. The critical issue for NASA regarding risk assessment is the fact that the radiation environment in space is a continuous flux of low doses from both low LET and high LET. Furthermore, the radiation environment is a mixed radiation field. This field is much different from that used as the basis for the current risk assessment models. Therefore it is crucial for NASA to have a basic understanding of the radiobiology involved with the types of radiation encountered in space and to develop accurate and precise radiation risk models for space travel. Currently there is an insufficient amount of data on HZE particles regarding biological effects to allow fully informed risk assessment.

1.1.3 Biological Effects of Space Radiation

A space shuttle mission in low earth orbit is estimated to give a dose of 0.1-4 mSv/day (Blakely 2000). ICRP recommends a dose limit for a radiation worker of 20 mSv/year

(Turner 1995). However biological differences will occur based on the radiation quality. The long-term biological effect that NASA is most interested in is cancer, a non-deterministic effect. More importantly, NASA puts a limit on the radiation risk to an astronaut from career radiation exposure of a 3% excess risk of cancer fatality (Cucinotta 2000). The basic question that NASA wants answered is what is the unique biological effect due to HZE particles of low fluence. Current preliminary research has shown that HZE particles lead to behavioral effects such as motor performance, premature aging, genomic instability, clustered DNA damage, cell cycle delays, cataracts and central nervous system damage (Worgul et al. 1989; Scholz et al. 1994; Goodhead 1995; Tsuboi et al. 1998; Blakely 2000; Shukitt-Hale et al. 2000; Smith et al. 2003). Due to the low fluence environment in space, the additional biological responses from non-targeted cells such as the bystander effect may prove to be important in the overall radiation risk assessment.

1.2 Linear Energy Transfer (LET)

As a heavy charged particle travels through matter it will deposit its energy largely by excitations and ionizations of atoms. Typically, a heavy charged particle will lose a small amount of its energy with a single electron collision, and therefore the path will be almost straight with only slight deflections. Unlike heavy charged particles, electrons and positrons will impart a large portion of their energy in a single electronic collision and will therefore have very torturous paths with great deflections. Additionally, both light and heavy charged particles can impart enough energy to oust an electron from the target material and that electron has enough energy to have its own path. These electrons are known as delta rays. For example, an iron particle of 1 GeV/nucleon can have a delta ray

16

with a track length of 800 μm, a large distance compared to a typical size of a cell of 10 μm (Chatterjee and Schaefer 1976).

To quantify the average linear energy loss of a charged particle in a medium over a given length, or in other words, the average ionization density along the direction of travel, the term linear energy transfer, LET, was coined. It describes the energy absorbed in the target in units of keV μm^{-1}. However it is important to note that when speaking of energy loss, it is not a continuous slowing down, but instead a discrete process and that LET only quantifies the average slowing down value. Also, the peak energy loss will occur at the end of the particle track, or range, as the particle is slowing down and picking up charge. For example, a 290 MeV/ nucleon carbon ion will have an LET of 13.6 keV/ μm, a 1 GeV proton will have an LET of 0.223 keV/ μm, and a 1 GeV/ nucleon iron ion will have an LET of 151 keV/ μm. In contrast, a 250-kVp x-ray beam will have an LET of 2 keV/ μm, based not on the x-ray beam since it is not charged but on the secondary particles that are formed. In this case, the x-rays or protons will be considered low LET, the carbon is medium LET, and the iron is considered a high LET ion. Again, these are averages on the macroscopic level. On the microscopic level, the energy deposited per unit length varies significantly over the track length.

Track structure depends greatly on LET. A high LET ion such as an iron ion of 1 GeV/ nucleon will have a thicker and shorter particle track compared to that of a low LET proton ion of the same energy. Fewer particles of high LET would be needed to give the same dose of 1 Gy compared to a low LET particle because the high LET particle will deposit this energy in a much shorter distance and has a dense formation of reactants along its track. Another issue is the delta rays. Often, the energy deposited in the medium

by these particles is not considered in the calculation of LET. However, delta rays are of low LET and as mentioned, have a torturous track path. Therefore, in reality, a heavy ion will have combined high LET and low LET components to its track.

1.2.1 Relative Biological Effectiveness

Relatively little has been determined regarding biological effectiveness of high LET radiation, partially due to the fact that ions of high LET other than alphas must often be produced in accelerators and are not as available as conventional x-rays. However, a few things are well established. For cell survival curves, for low LET radiation, a repair shoulder is visible in the low dose region but for high LET radiation, the survival curve is a straight line, with no repair region (Hall 2000). This is stating that high LET radiation is more effective at causing cell death than low LET radiation and that at the low doses no repair is seen. It has also been shown that high LET radiation is more effective at mutagenesis and chromosome aberrations compared to low LET radiation (Ritter et al. 1992; Masumura et al. 2002). Other findings include induction of more complex clustered lesions at high LET radiation (Sutherland et al. 2001). This is based on the fact that high LET radiation interacts with DNA directly compared to indirectly for low LET.

When speaking of risk from high LET radiation, the relative biological effectiveness (RBE) ratio is used. It is a ratio between the dose of the low LET radiation, i.e. x-rays, compared to the dose needed of high LET radiation that would give the same biological effect. RBE is dependent on LET, dose rate, dose fractionation, and the endpoint used. Generally, RBE increases with LET, mainly due to the track structure

18

associated with heavy ion particles or, simply, high LET radiation is more effective at biological damage that is less repairable than low LET radiation.

In addition to looking at risk through the RBE, quality factors have also been set for different radiation types. High LET radiation is known to be more effective at damaging a biological system per unit dose, and to quantify the effectiveness of different radiation types the International Committee on Radiological Protection (ICRP) have incorporated the quality factor, Q. The Q value is essentially like an RBE, where it takes into consideration the effectiveness at producing biological damage from different types of radiation. Also, the commission introduced the dose equivalent value that incorporates different radiation qualities by multiplying the dose in Gy by Q and ending in units of Sv. The Q value is dependent on LET, where the Q value for x-rays is 1 but for a heavy ion of LET such as iron, the Q value is between 10-20 (Turner 1995). Dose equivalent has been a measure for radiation protection and radiation limits are set for occupational workers using it. However, knowledge of the biological effects of high LET radiation is limited due to the lack of high LET radiation facilities on earth, and therefore the models used for Q values of high LET are in constant debate and in need of additional support from traditional biology. More specifically, for NASA the uncertainties related to space radiation and related biological effects raises difficulties in determining Q values and radiation risks associated with the high LET components of space. Several issues then arise. In space, radiation is present in low fluences but all the time and is a combination of all types. How does one assign a Q value or a radiation risk to a small population of cells receiving low doses of different radiations? When speaking of dose in space, one speaks on a macroscopic level where it is low to the entire population but on the

microscopic level the dose is significant to a small portion of the population. More so, with the possibility of the bystander effect contributing potentially additional damage to cells not traversed by radiation, radiation risk and models will need to be reevaluated for space travel.

1.3 Bystander Effect

Traditional cell damage is currently based on the theory that a cell is damaged only if radiation traverses the cell. Damage to the DNA can include base damage, single strand breaks, double strand breaks, and crosslinks within the DNA. Also, damage to the cell can be shown through activation of specific proteins, serious chromosomal damage such as micronuclei formation or chromatin bridges, cell cycle arrest, or cell death via apoptosis or necrosis when damage cannot be repaired. It has been traditionally thought that damage must occur to the nuclear DNA in order to have cell damage. However, in the past decade, there has been evidence by several independent research groups that indicates higher damage within cell cultures than expected based on the number of cells traversed by the radiation, and the term-bystander effect has been coined (Mothersill and Seymour 1997; Nagasawa and Little 1999; Lyng et al. 2000). The bystander effect is the observation that non-irradiated cells near a cell traversed by radiation also express biological responses such as double strand breaks, micronuclei, genomic instability, and cell cycle arrest. The bystander effect was first shown by Nagasawa and Little when they irradiated only 1% of the cell population with α-particles but saw chromosome damage via sister chromatid exchanges in up to 30% of the cell population (Nagasawa and Little

1992). Since then, other instances of the bystander effect have been characterized using the medium transfer method, gap junction dependency, or microbeams.

1.3.1 Medium Mediated and Gap Junctions

Mothersill and Seymour *et al.* showed that by transferring medium from low LET irradiated cells to non-irradiated cells, the non- irradiated cells had an increase in cellular damage (Mothersill and Seymour 2001). They concluded that some factor is being transferred from the irradiated cells into the medium, which is causing an effect in the non-irradiated cells. Another instance of medium mediated bystander effect has been shown using the insert system (Yang et al. 2005). Unirradiated bystander cells were shown to have an increased induction of micronuclei when sharing medium with cells that were irradiated with 250 kVp x-rays.

Another experiment done by Mothersill and Seymour *et al.* looked at the role of cell-cell contact. Connexin proteins, which make up the gap junctions, pass ions, second messengers and small metabolites between cells that are in contact such as confluent cells. The experiment was performed using a GJIC (gap junction intercellular communication) inhibitor. They showed that by inhibiting the gap junctions, the bystander effect did not decrease (Mothersill and Seymour 1998). Contrary to the data of Mothersill and Seymour, Azzam and Little *et al.* showed that inhibition of gap junctions in their cell line did decrease the bystander effect (Azzam et al. 1998). Since gap junctions are too small to pass proteins, it has been hypothesized that perhaps the bystander effect is an emission of reactive species into the medium. Although the exact nature of the bystander effect is unknown, it has been shown that in some cell lines, it is passed through gap junctions, and in others, it is present in cells with no cell-to-cell

contact and is medium mediated. Also it has been shown that by targeting only the cytoplasm of radioresistant glioma cells using a microbeam, a bystander effect was seen (Wu et al. 1999; Shao et al. 2004). One important characteristic of the bystander effect is that there is no threshold at which the bystander effect starts. It appears to be present at the lowest doses tested (Ballarini et al. 2002). The bystander effect is most likely a combination of various factors, dependent on cell type and intercellular communication. It has been shown to be dependent on reactive oxygen species such as hydrogen peroxide and superoxide, cytokines, transforming growth factor $\beta1$, or perhaps a combination of the above (Lyng et al. 2000).

There is a debate as to whether the bystander effect is a biological defense mechanism or an enhancement of cell death. A commonality from all the bystander effects that have been recorded is the fact that most responses are evident at low doses and saturate after 0.5 Gy. If the damaged cells release a factor into the medium, perhaps it is to enhance cell killing in order to protect against the possibility of carcinogenic damage due to the surrounding radiation changes. Another possibility is that this is a negative effect, and that critical cells are killed. Regardless of whether the bystander effect is a positive or negative mechanism, it is occurring and detailed studies of the mechanisms involved are needed.

1.3.2 Heavy Ions and Bystander Effect

Currently little is known regarding biological effects from high doses of heavy ions, let alone to be able to understand risks from low doses. To date, little work has been done with heavy ions and the bystander effect. There have been published data of the

bystander effect by Shao *et al.* with carbon ions. The group showed a micronuclei bystander response after 13 keV/μm and 100 keV/μm carbon ions in human salivary gland neoplastic cells (Shao et al. 2002). Additionally, they showed that with the addition of a NO scavenger, PTIO, the bystander effect was eliminated after 100 keV/μm carbon ions in these cells. The group also looked at the role of gap junctions in human fibroblasts AGO1522 after a 290 MeV/nucleon carbon ion beam of LET 100 keV/μm (Shao et al. 2003) (Shao et al. 2003). They grew AGO1522 cells to confluency and inhibited gap junctions with lindane and found the MN bystander effect decreased considerably but not completely. Similarly, they added cAMP, which is an enhancer of GJIC and saw somewhat of an increase of the low dose bystander response.

The purpose of this project is to characterize the induction of the bystander effect from heavy ions, specifically iron, as will be encountered in space. Comparison of biological responses after low LET 250 kVp x-rays will be made with the 1 GeV/nucleon iron ions of high LET. Endpoints that were explored included micronuclei formation, chromatin bridges, p21^{wafl} expression, and cell cycle changes in human keratinocyte cells. Also, data will be presented that show the induction of the bystander effect signaling from two different cell lines, fibroblasts and keratinocytes, from both beams in the form of micronuclei and p21^{wafl} induction. The reasoning behind mixing cell lines is the eventual movement to studies of bystander induction in tissues composed of these two cell lines, a more *in vivo* approach. All bystander induction is represented as a form of medium mediated response using the insert system.

Chapter 2

Materials and Methods

2.1 Materials

The two cell lines used are the hTERT immortalized keratinocytes (Dickson et al. 2000)

and the AGO1522 normal human skin diploid fibroblasts which were obtained from

Genetic Cell Respository at the Coriell Institute for Medical Research (Camden, NJ,

USA). Both cell lines have wild-type p53. The keratinocytes were grown in 37°C in 95%

air and 5% CO_2 with Keratinocyte-SFM (Gibco) supplemented with 100 U/ml penicillin,

0.1% of 0.3 mM $CaCL_2$, L-glutamine, epidermal growth factor, and bovine pituitary

extract. AGO1522 cells were grown in 37°C in 95% air and 5% CO_2 with α-modified

MEM (Sigma) supplemented with 20% fetal bovine serum (FBS, Hyclone), 100 μg/ml

streptomycin and 100 U/ml penicillin. When the AGO1522 cells were used during

experiments, the medium was changed to the keratinocyte medium. All AGO1522

experiments were initiated by the addition of Trypsin and re-plating confluent cells at

numbers of $5x10^4$-$1.3x10^5$, depending on the time of assay. Keratinocytes differentiate

once confluent and therefore were kept at low cell densities to ensure that by the time of

assay cells had not grown to confluency. Therefore all plating with keratinocytes was

done in stable exponential growth. All plating for experiments was done 24 hours prior to

irradiation. For studies at Brookhaven National Laboratory, cells were transported and given at least 1 day in the incubator to restabilize the pH and temperature prior to plating for heavy ion beam irradiation.

The bystander studies were performed in an insert system as shown below in Figure 2-1. Cells were plated in wells of a 6 well dish (Falcon) with growth area of 9.6 cm^2 per well and a companion transwell culture dish (Falcon) with a growth area of 4.2 cm^2. The inserts have a membrane with pores of 1.0 μm at a density of $1.6 \times 10^6/cm^2$ to allow passage of molecules. Using this system, cells plated in the dish are those that are irradiated and immediately after irradiation inserts were placed into the wells, serving as the bystander cells. Therefore, medium passed between bystander and directly irradiated cells, but a distance of 0.9mm separated the cells.
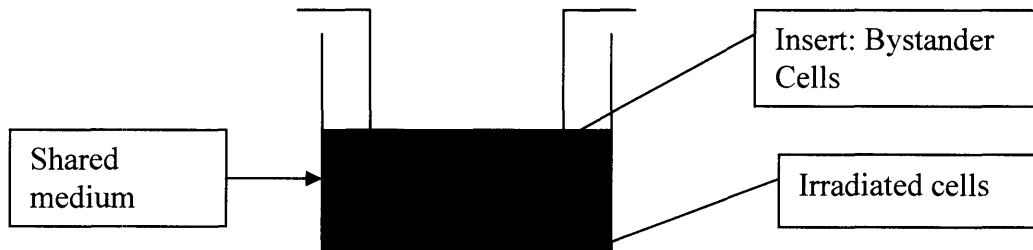
Figure 2-1: **Schematic of the transwell insert co-culture system.**

2.2 Cell Irradiation

Prior to irradiation, fresh medium was added to each well and insert only for x-rays. Due to the setup for the iron beam, all media was aspirated prior to irradiation. Irradiations were performed at room temperature using a 250 kVp X-ray machine (Siemens Stabilipan 2) at Massachusetts General Hospital at a dose rate of 2.08 Gy/min. The 1

25

GeV/nucleon Fe beam of LET of 151 keV/μm irradiations were performed at the NASA

Space Radiation Laboratory (NSRL) located in Brookhaven National Laboratory, Upton,

NY with dose rates ranging from 0.05 Gy/min to 2 Gy/min. The Bragg curve for 1

GeV/nucleon was obtained from Dr. Adam Rusek, physicist at NSRL, and is shown in

Figure 2-2. The Bragg curve is obtained through a thickness in plastic of equivalent

density of tissue.
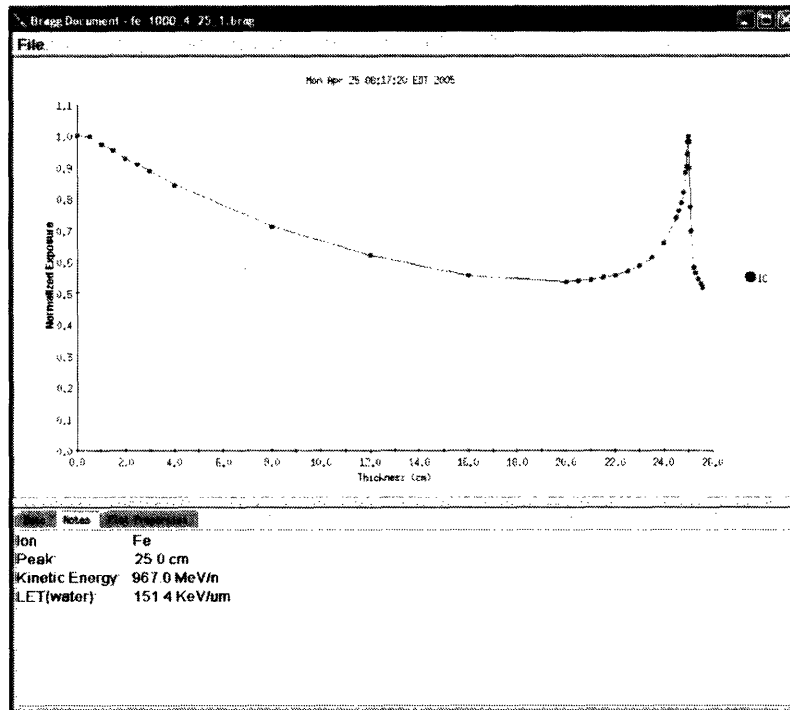
Figure 2-2: **Bragg curve for 1 GeV/nucleon Fe ions**. Horizontal axis is distance in water traveled by a particle.

Since the Fe ion beam traveled through mostly air and a little bit of the plastic of the

wells, the irradiation is performed over the beginning of the Bragg curve where it is linear

over that region and little loss in energy or LET occurs through the sample. Figure 2-3

shows the holder, darker edges, and the wells on a CCD camera picture taken during

irradiation with 1 GeV/nucleon Fe ions. The beam comes perpendicular, out of the page.
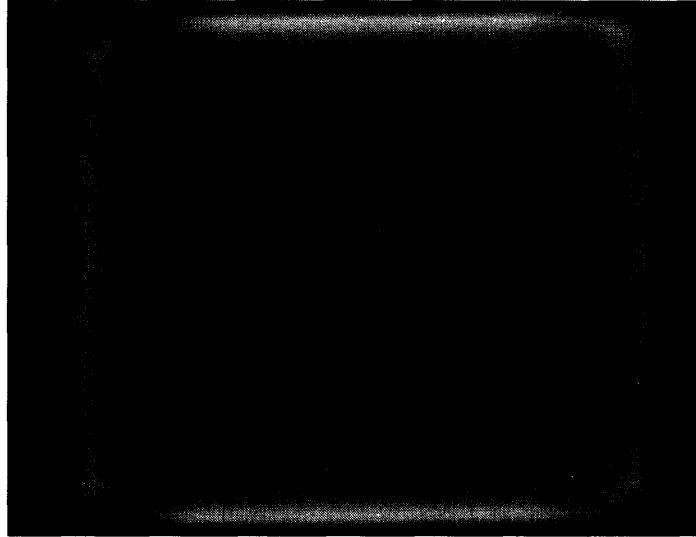
Figure 2-3: **CCD camera picture of experimental setup for heavy ion irradiation.**
Obtained with 1 GeV/nucleon Fe ion irradiation. Photograph shows 2 6-well plates held
in place perpendicular to the beam by a plastic holder, shown as dark outlines around the
well plates.

At NSRL, dose is calculated using ionization chambers. Ionization chambers essentially

are two parallel plates in a gas filled chamber attached to a voltage source. When

radiation passes through the gas chamber, it ionizes the gas and the particles travel to the

plates and create a voltage drop, which is recorded (Knoll 1999). Ionizing chambers are

used to count the number of particles that pass through the chamber, hence the fluence of

the beam. To calculate dose in air, the simple expression can be used:

$$\dot{D} = \dot{\phi}\left(-\frac{dE}{\rho dx}\right)$$ 2-1

where the dose rate is equal to the fluence rate times the stopping power divided by the

density of the material. The ionization chamber gives the fluence rate. The difference

between requested dose and delivered dose for the Fe ion beam never exceeded 2% and

therefore no error bars are seen on the dose axis, for the error is smaller than the points.

Immediately after irradiation, inserts were placed in the wells and cells were co-cultured together in the incubator until time of fixation. Controls were also treated in the same manner, without irradiation. All bystander samples were done in the 6 well plate and insert system, but cell cycle analysis was done in cells in T75 flasks.

2.3 Micronuclei and Chromatin Bridge Assay

A micronucleus is a chromosome fragment that is not included with the rest of the nucleus at cell division. It has enough information to form its own nuclear membrane and looks like a mini nucleus in the cytoplasm. The rate of micronuclei (MN) formation after both types of irradiations was determined by two methods. The first was using the cytokinesis-block technique(Fenech and Morley 1986). After placing inserts into the companion wells, cytochalasin B (Sigma) was added to the co-culture to a final concentration of 0.5 µg/ml. After 72 h, cells were fixed in methanol:acetic acid (3:1 v/v). After allowing the samples to dry, cells were stained with the nuclear stain 4', 6'-diamidimo-2-phenylindole (DAPI) solution (10 µg/ml in water). Cells then were mounted with FluoroGuard™ Antifade reagent (Bio-rad) to preserve the fluorescence stain. Micronuclei were scored under a fluorescence microscope in only binucleated cells. At least 500 cells were scored from at least 10 view fields. In the second method no cytochalasin B was added and cells were fixed 24 h after irradiation. The staining and counting procedure remained the same. For the AGO1522/Keratinocyte and vice versa bystander co-culture samples, cytochalasin B was not used due to toxicity issues arising from concentration differences of the chemical for the two cell lines. Instead samples were fixed 24 hours after irradiation and stained and counted as described above.

Another type of chromosomal damage that became apparent in the keratinocytes is chromatin bridges. During cell division, the duplicated DNA in the cell is condensed to identical copies of chromosomes. In mitosis, the phase when the chromosomes get separated and are pulled apart is known as anaphase. Usually, each chromosome is pulled apart by equal force and each daughter nucleus gets the identical chromosomes. However, it has been shown that from various toxins such as cigarette smoke, UV light, and radiation, during anaphase, while the two chromosomes are being pulled apart, instead the chromosomes continue to fuse together forming a chromatin bridge between the two daughter cells (Gisselsson et al. 2000; Thomas et al. 2003). The final appearance has two separated nuclei with a string of various lengths and thickness of chromatin connecting them together. Chromatin bridges were counted using the same procedure outlined above for micronuclei without cytochalasin B. Cells were fixed 24 hours after irradiation and stained with DAPI.

2.4 p21$^{\text{Wafl}}$ Immunofluorescence

It has been well documented that after UV or ionizing radiation, cells with wild-type p53 respond by increasing p53 levels which in turn arrests the cells until damage is repaired or triggers the cells to programmed cell death called apoptosis (Concin et al. 2003). p21$^{\text{wafl}}$ is a direct downstream response protein of p53 that is involved in cell cycle arrest. Therefore, p21$^{\text{wafl}}$ induction is an indication that p53 was activated.

Immunofluorescent staining as summarized here is previously described by Azzam *et al.*, 2001 and was analyzed at various time points after irradiation for the iron beam but at 24 hours after x-rays (Azzam et al. 2001). The timing of 24 hours was

determined as the peak response of p21^{waf1} after a 2 Gy irradiation with x-rays by a time course curve (data not shown). At the time of staining, cells were rinsed in PBS supplemented with 1 mM $MgCl_2$ and 0.1 mM $CaCl_2$ (PBS+), then fixed in 3% (v/v) paraformaldehyde in PBS+ for 30 minutes. After a 5 minute rinse with 50 mM NH_4Cl and two rinses with PBS+, the cells were permeabilized in ice cold Triton X buffer consisting of 50 mM NaCl, 3 mM $MgCl_2$, 200 mM sucrose, 10 mM HEPES, pH 7.4, and 0.5% Triton – 100 in water. After three rinses with PBS, cells were blocked in 10% goat serum for 20 min and then incubated in p21^{waf1} mouse monoclonal antibody (Oncogene) for 1 h and then stained with Alexa 488 goat anti-mouse IgG secondary antibody (Molecular Probes) for 45 min at room temperature. Cells were then washed at least twice with PBS before staining with DAPI (Sigma) for 2 minutes and followed by two washes with PBS. Cells were mounted with FluoroGuard™ Antifade reagent (Bio-rad) to preserve the fluorescence stain. At least 500 cells were counted from at least 10 fields of views.

2.4 Cell Cycle Assay

Cells go through a cell cycle consisting of four phases: G1, S, G2 and mitosis. It has been well documented that if cells are damaged via radiation, the cells will arrest in G1 via p53 or G2 and will not proceed through the cell cycle until damage is repaired. If damage is not repaired, cells will go into apoptosis, necrosis or permanent cell cycle arrest.

Cell cycle analysis was performed on directly irradiated keratinocytes to compare cycle delays from x-rays and iron ions. Cells were seeded 24 hours prior to irradiation in T75 flasks with cell densities that would ensure at least $2x10^6$ cells on the day of processing. This cell density was not confluent. Cells were processed 5, 24, and 48 h after

irradiation for x-rays and 5, 24, 40, and 50 h post iron irradiation. At the time of processing, cells were trypsinized, collected, and washed twice with PBS. Cells were then vortexed to maintain single cell suspension and fixed in 100% ice-cold ethanol at least overnight. Cells were then rinsed again in PBS and stained with 0.5 mg/ml RNase (Sigma), 0.1 mg/ml Propidium Iodide (PI) (Sigma), 0.1% NP40 (Sigma) detergent in PBS for a total of 0.5 ml working volume. Cells were then analyzed for DNA content using the flow cytometer FACScalibur (Becton Dickson, Franklin Lake, NJ USA) with the software CellQuest V5.1 Mac OS X.

2.5 Colony Formation Assay

Clonogenic assay was performed to obtain survival curves for directly irradiated keratinocytes. Cells were plated in T25 flasks at 300 cells/flask for x-ray doses of 0-0.5 Gy, 450 cells/flask for 1 Gy, 600 cells/flask for 2 Gy, and 3000 cells/flask for 3 Gy and 5 Gy. After 24 hours, cells were irradiated with x-rays and then incubated for 10-12 days. Colonies were fixed in methanol and stained with methylene blue. Colonies containing at least 50 cells were counted. For x-rays, the linear-quadratic model with the equation $SF=\exp(-\alpha D-\beta D^2)$ and for the Fe ion beam the linear equation $SF=\exp(-\alpha D)$ was used where D is dose in Gy, and α and β are constants.

2.6 Statistical Analysis

All data shown here are from at least three or more separate experiments, unless otherwise noted. All results are recorded as means ± standard error. Statistical comparison of the groups and controls was done using SigmaPlot 2001 software.

Chapter 3

Results

3.1 Cell Survival

To see the relative biological effectiveness between 250 kVp x-rays to 1000

MeV/nucleon Fe ion beam, standard survival curves were obtained and are shown in

Figure 3-1.
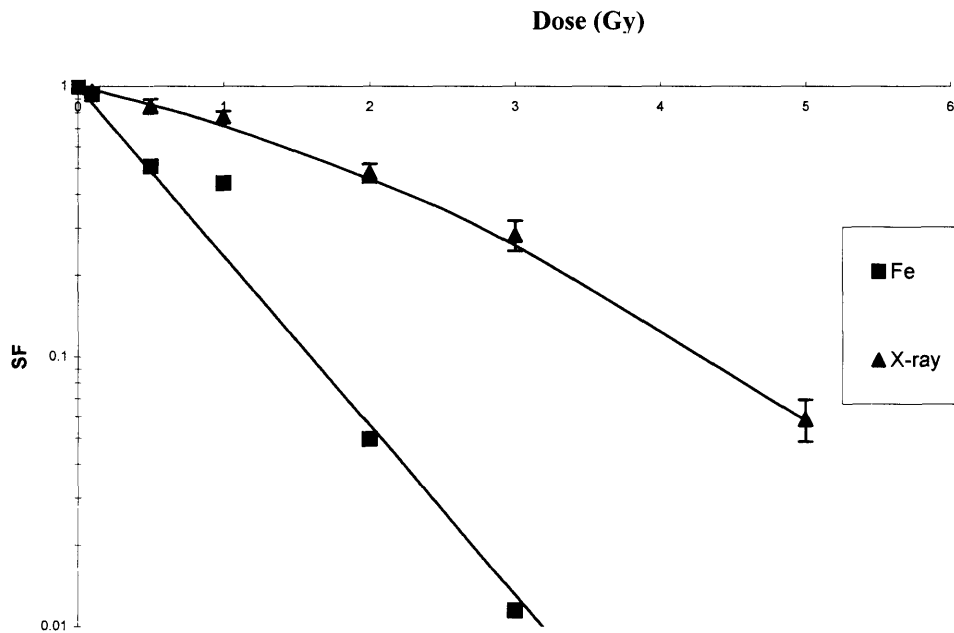
Figure 3-1. **Survival Fraction of keratinocytes**. Horizontal axis is dose (Gy). X-ray data
(▲) are the means of three independent experiments ± s.e and fit with the curve
SF = exp (-0.276D -0.0587D^2). Fe ion data (▪) are from one experiment and fit with the
curve SF = exp (-1.44D).

The iron curve is based only on one experiment and therefore has no error bars. The x-ray curve showed a typical repair shoulder, whereas the Fe curve showed a steep linear decrease, as usually noted with low and high LET radiations. For iron, the equation that characterizes the curve is SF = exp (-1.44D) and for the x-rays SF = exp (-0.276D - 0.0587D^2).

3.2 p21^{wafl} Expression

Expression of the protein p21^{wafl} in keratinocytes was determined both in directly irradiated cells and bystander cells. In Figure 3-2, p21^{wafl} induction is seen using a fluorescent labeled antibody in keratinocyte cells and compared visually between control and directly irradiated cells 24 h after 2 Gy of 250 kVp x-rays. Figure 3-3 shows the 24 h p21^{wafl} induction in bystander keratinocyte cells co-cultured with control and directly irradiated keratinocyte cells with 2 Gy x-rays. All of the samples shown were stained at the same time and under the same conditions.
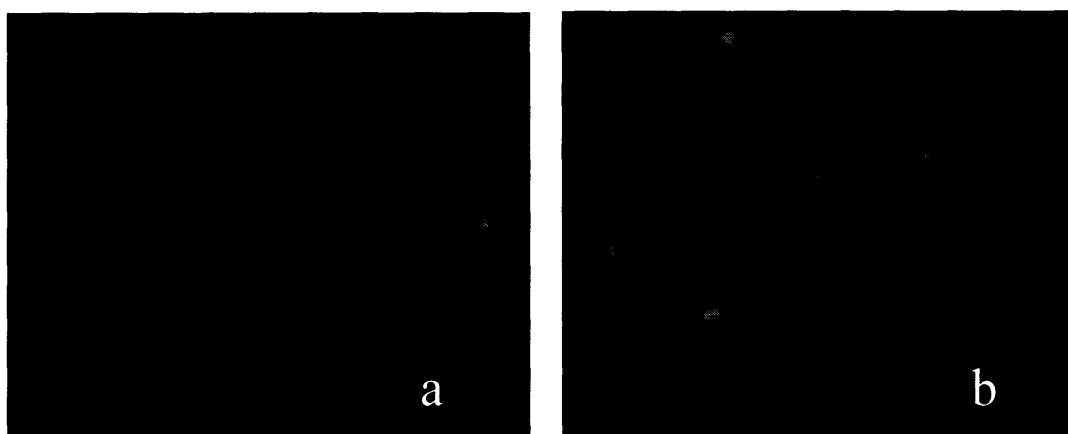
Figure 3-2: *In situ* immunofluorescence detection of p21^{wafl} in keratinocytes 24 h after x-ray irradiation. (a) unirradiated cells; (b) cells directly irradiated with 2 Gy x-rays.
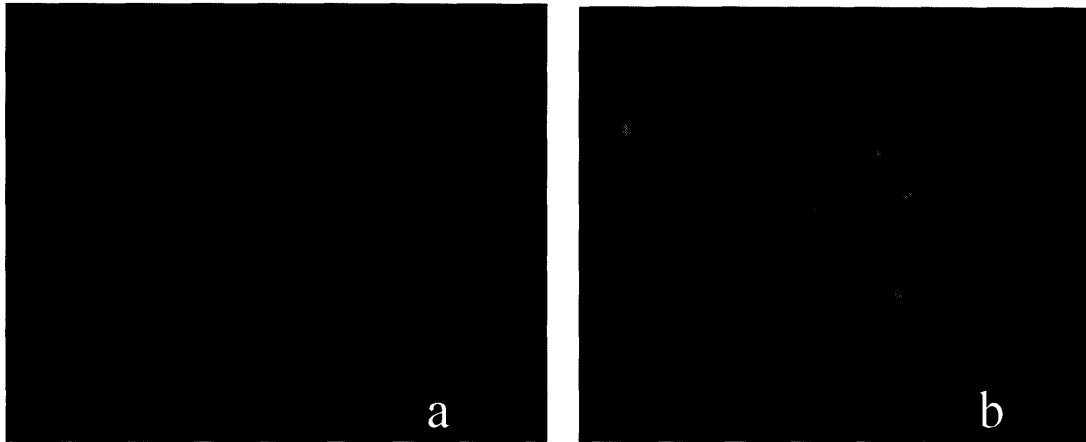
Figure 3-3: *In situ* **immunofluorescence detection of p21^{wafl} in bystander keratinocytes 24 h after x-ray irradiation.** (a) cells co-cultured with unirradiated cells; (b) bystander cells co-cultured with cells irradiated with 2 Gy x-rays.

Keratinocytes were fixed 24 hours after x-ray irradiation because this was found to be the time of maximum p21^{wafl} induction in keratinocytes from a time course. However it was seen that from iron irradiation, p21^{wafl} expression did not appear until 40-50 h after irradiation, showing at least a 24 h delay compared to x-rays. Figure 3-4 shows induction of p21^{wafl} in both directly irradiated and bystander keratinocytes 24 hours after x-ray irradiation and Figure 3-5 quantitatively shows induction 40-50 h after iron irradiation. A two-fold increase in percentage of cells having p21^{wafl} induction in the bystander cells was seen for both x-rays and Fe ion beam. Also, a typical plateau in the effect was noted in both. For directly irradiated cells, the Fe ion beam showed a much larger increase in percentage of cells expressing p21^{wafl} expression. For a 2 Gy irradiation, the p21^{wafl} induction from x-rays on average was 25% of the cells where as with iron ions it reached 40%.
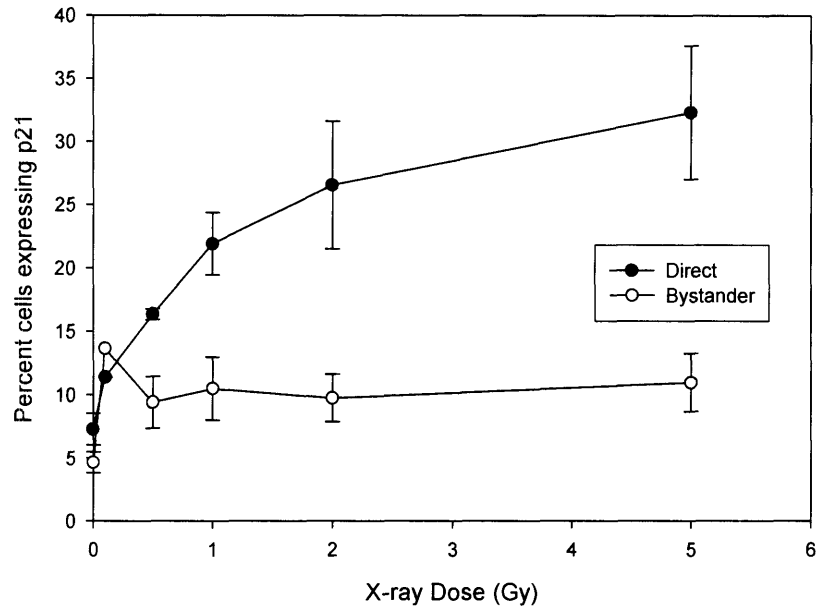
Figure 3-4: **Dose response for induction of p21^{wafl} in directly irradiated and bystander keratinocyte cells 24 h after x-ray irradiation.** Results are the means of at least three independent experiments ± s.e.
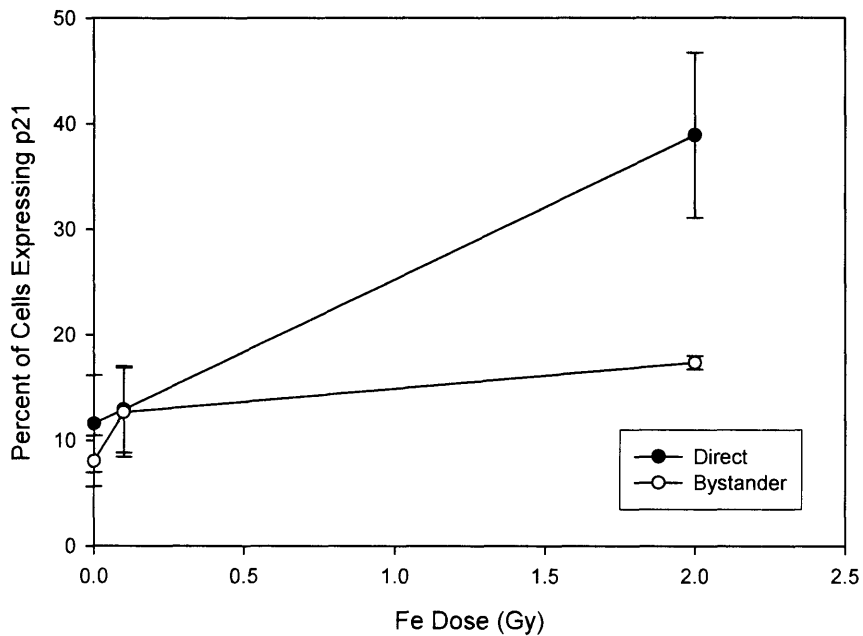
Figure 3-5: **Dose response for induction of p21^{wafl} in directly irradiated and bystander keratinocyte cells 40-50 h after Fe ion irradiation.** Results are the means of at least three independent experiments ± s.e.

After seeing a bystander p21^{wafl} induction from keratinocytes co-cultured with

keratinocytes, the bystander effect from directly irradiated human fibroblasts, AGO1522

cells, co-cultured with bystander keratinocytes via p21^{wafl} induction was tested, and data

are shown in Figure 3-6. The curve is based only on two experiments, and therefore the

error bars represent range and not standard error. A typical plateau is seen by 1 Gy, and a

two-fold increase in percentage of cells showing p21^{wafl} induction in the bystander

keratinocyte cells is noted.
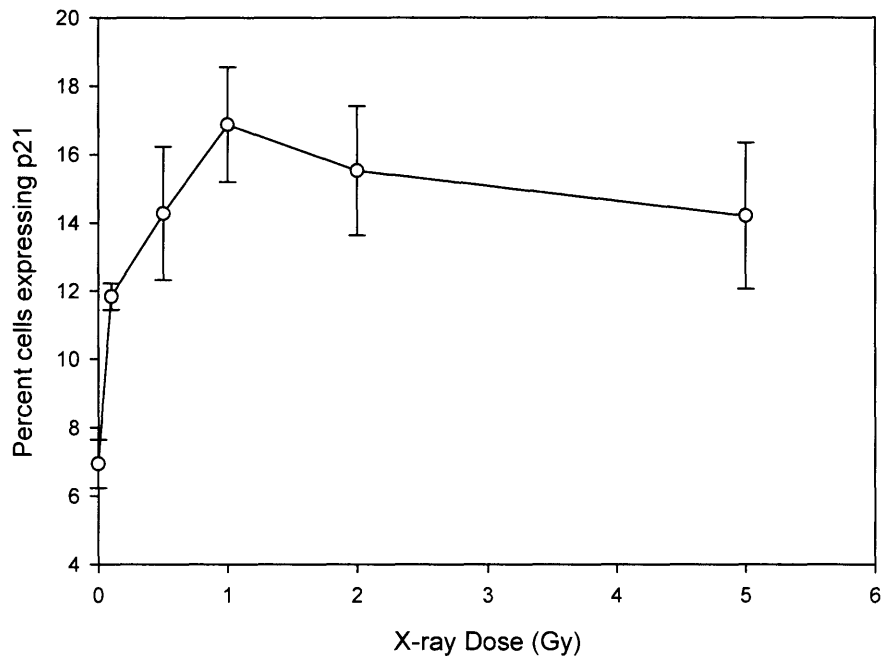
Figure 3-6: **Dose response for induction of p21^{wafl} in bystander keratinocyte cells co-cultured with AGO1522 cells for 24 h after x-ray irradiation.** Data are the averages of two experiments and error bars represent the range.

3.3 Cell Cycle Delays

Noting the fact that radiation is known to induce a cell cycle arrest, a possible explanation

for the delay in p21^{wafl} expression after Fe irradiation is a G2 cell cycle delay in

keratinocytes after Fe ion irradiation compared to that x-rays. Cell cycle analysis was conducted in cells at 5, 24, 40, and 50 h after irradiation with Fe ion beam and at 5, 24, and 48 h after x-rays. For x-rays at 5 h, only one experiment was preformed and therefore no error bars are shown and the 24 h and 48 h results are based only on two experiments. Figures 3-7,8,9 show cell cycle analysis after x-rays and figures 3-10,11,12,13 show data from Fe ion irradiation. As seen, a slight G2 arrest is noted in the keratinocytes 5 h after 2 Gy of x-ray irradiation and then is gone by 24 h. No significant differences are measurable at 0.5 Gy. However, for Fe irradiation, cell cycle delay at G2 is maintained from 5 h until 50 h along with a decrease in G1 and S cells, due to the holding of cells at G2 at 2 Gy. Similar trends are seen at 0.5 Gy, although the magnitude is less.
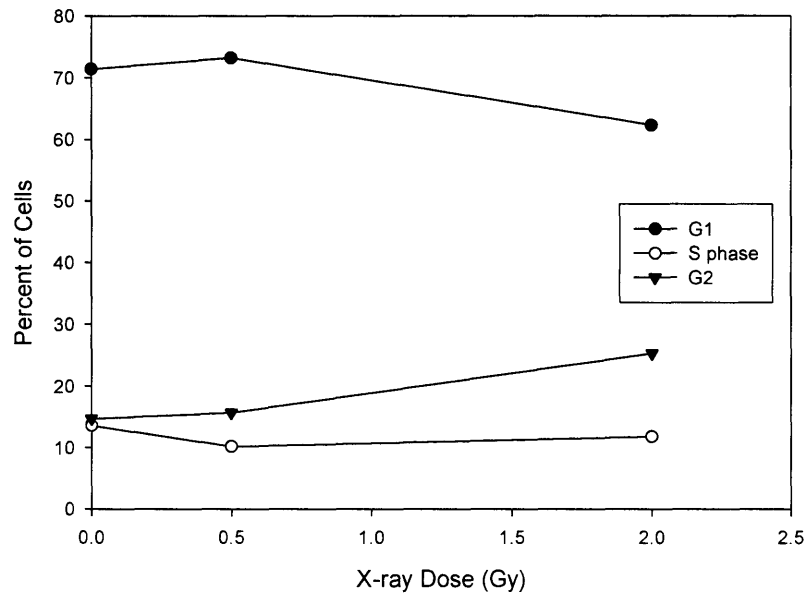
Figure 3-7: **Cell cycle distribution in directly irradiated keratinocyte cells 5 h after x-ray irradiation**. Data are based on one experiment.
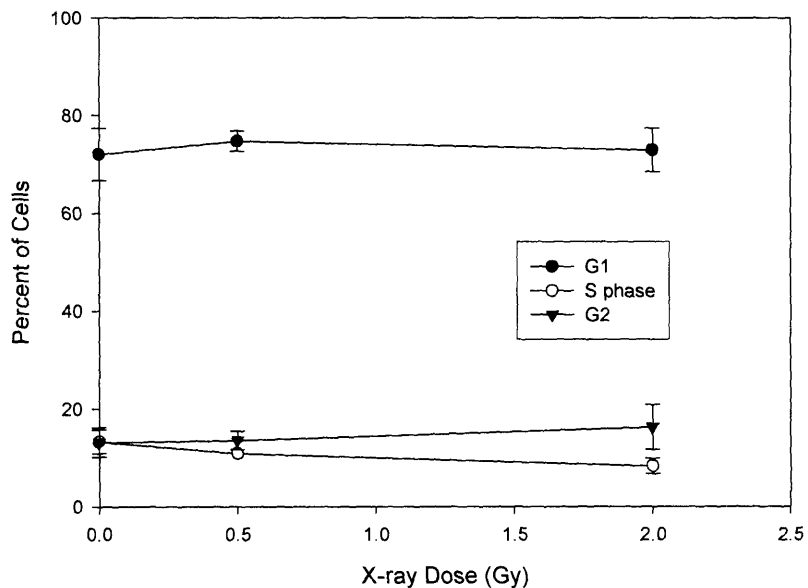
Figure 3-8: **Cell cycle distribution in directly irradiated keratinocyte cells 24 h after x-ray irradiation**. Data are the averages of two experiments ± range.
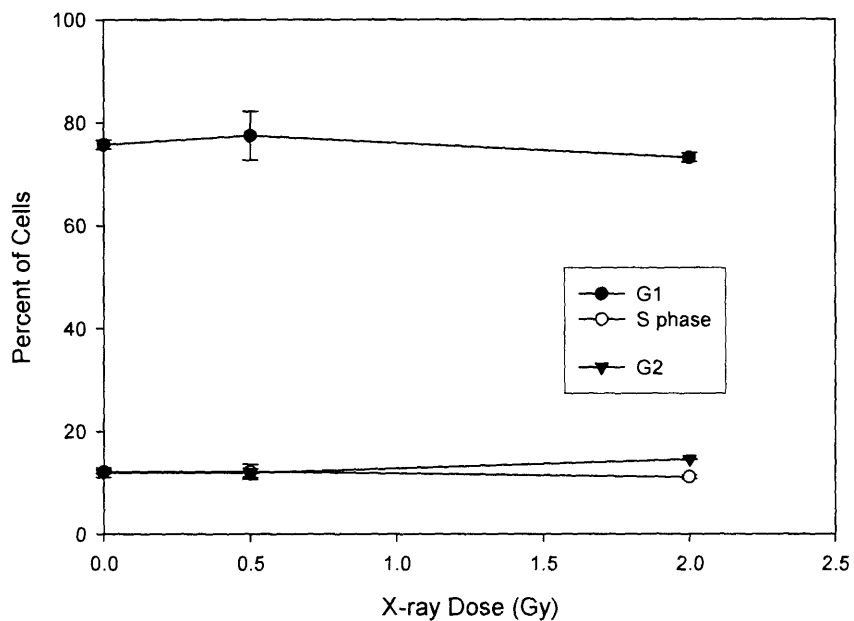
Figure 3-9: **Cell cycle distribution in directly irradiated keratinocyte cells 48 h after x-ray irradiation**. Data are the averages of two experiments ± range.
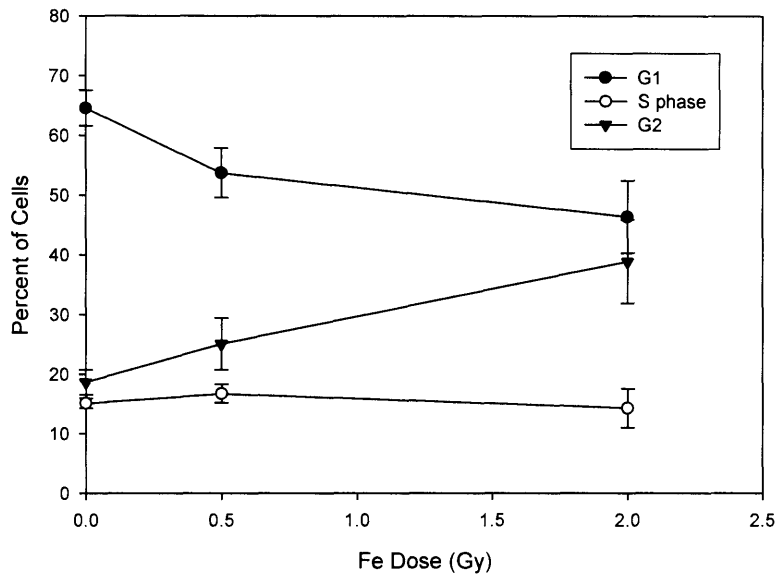
Figure 3-10: **Cell cycle distribution in directly irradiated keratinocyte cells 5 h after Fe ion irradiation.** Data are the means of at least three experiments ± s.e
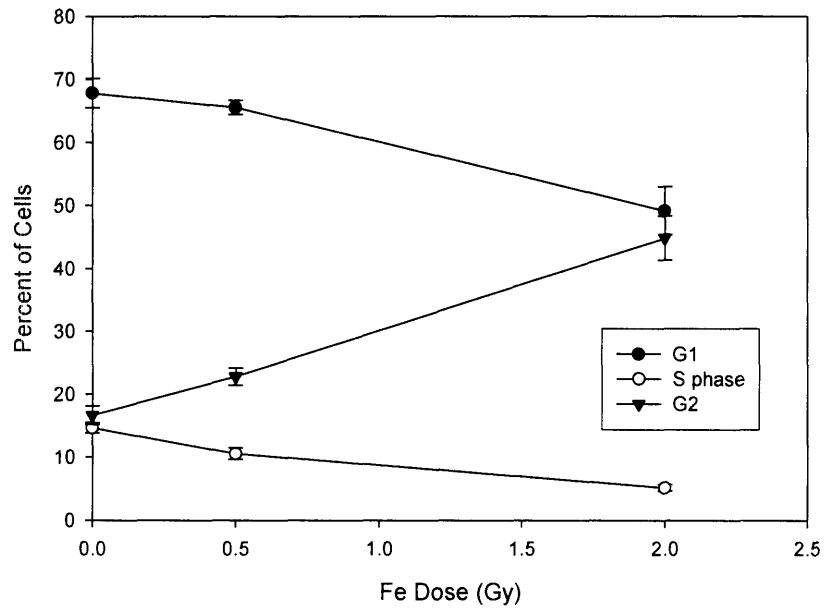
Figure 3-11: **Cell cycle distribution in directly irradiated keratinocyte cells 24 h after Fe ion irradiation.** Data are the means of at least three experiments ± s.e
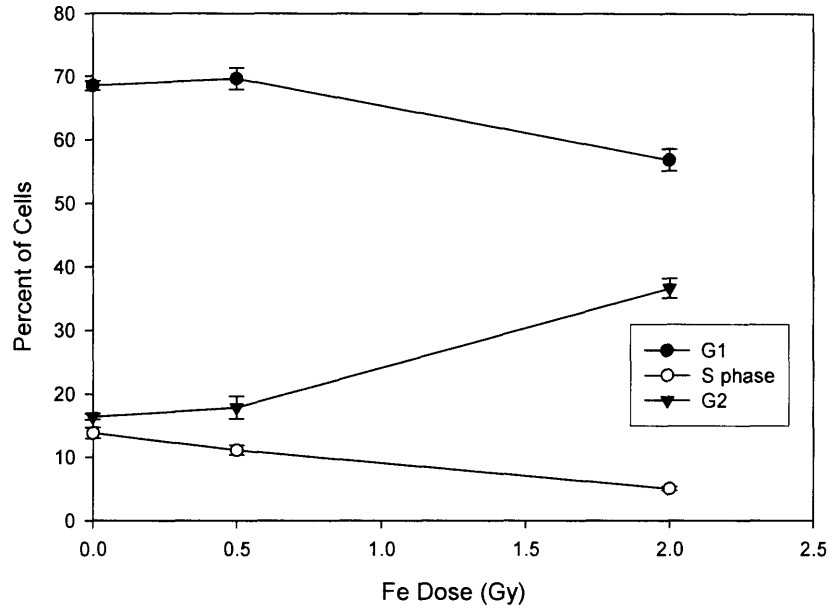
Figure 3-12: **Cell cycle distribution in directly irradiated keratinocyte cells 40 h after Fe ion irradiation.** Data are the means of at least three experiments ± s.e
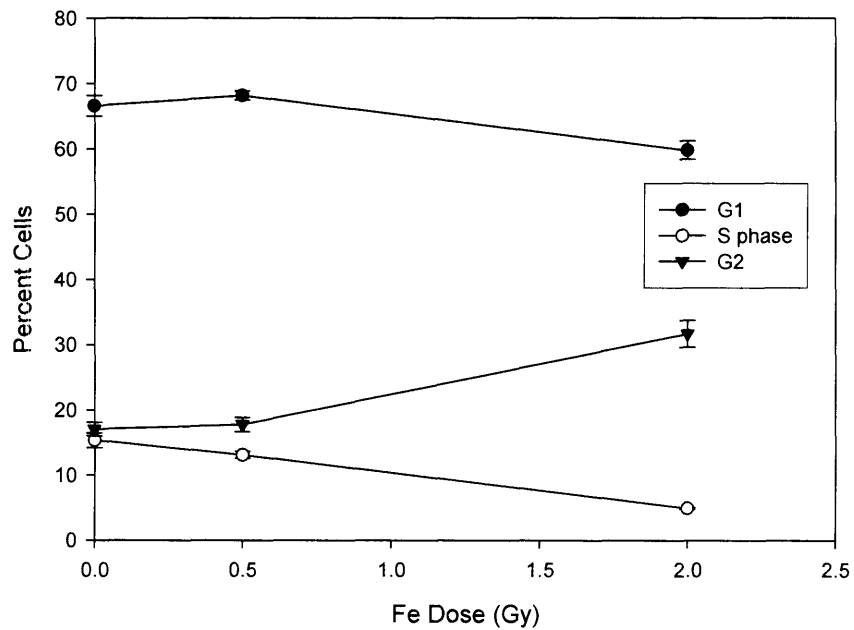
Figure 3-13: **Cell cycle distribution in directly irradiated keratinocyte cells 50 h after Fe ion irradiation.** Data are the means of at least three experiments ± s.e

3.4 Micronuclei Formation

For micronuclei induction, to insure that the micronuclei counted are from the parent cell and not the daughter cell, in the generally used protocol, cytochalasin B is added to halt the cells in a binucleated form (Nilsson et al. 1973). However, it was noticed that when adding cytochalasin B to keratinocytes and scoring for MN, no bystander response was seen after x-rays. Although, when the cells were fixed 24 hours after irradiation and no cytochalasin B was used, a bystander effect was seen. Figure 3-14 shows directly irradiated nuclei of cells that received 2 Gy of x-rays and there is noticeable MN formation, without cytochalasin B in cells fixed 24 hours after irradiation. Figure 3-15 shows two experiments of MN induction with and without cytochalasin B. It is seen that the direct curves are similar, with the addition of cytochalasin B decreasing the number of MN slightly. However, it is clearly seen that no bystander effect is present with cytochalasin B, although without cytochalasin B a typical plateauing curve is observed with a two-fold increase in this bystander response. Although only one curve is shown for each experiment, repeats have been done and consistently showed the lack of the bystander effect with the addition of cytochalasin B and presence of the bystander effect without the addition of cytochalasin B.
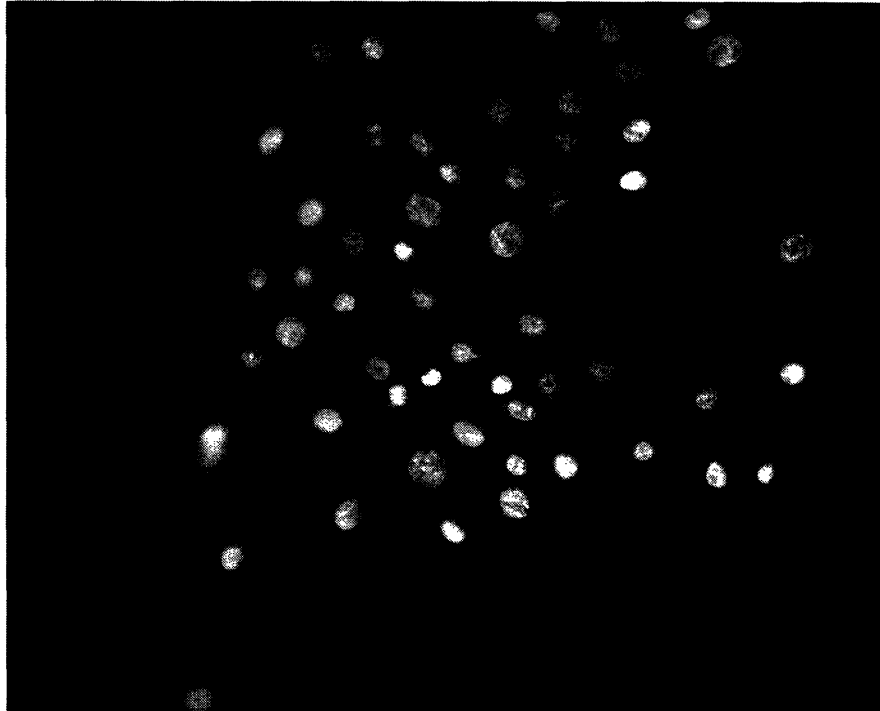
Figure 3-14: *In situ* fluorescence detection of micronuclei in directly irradiated keratinocyte cells 24 h after 2 Gy x-ray irradiation.
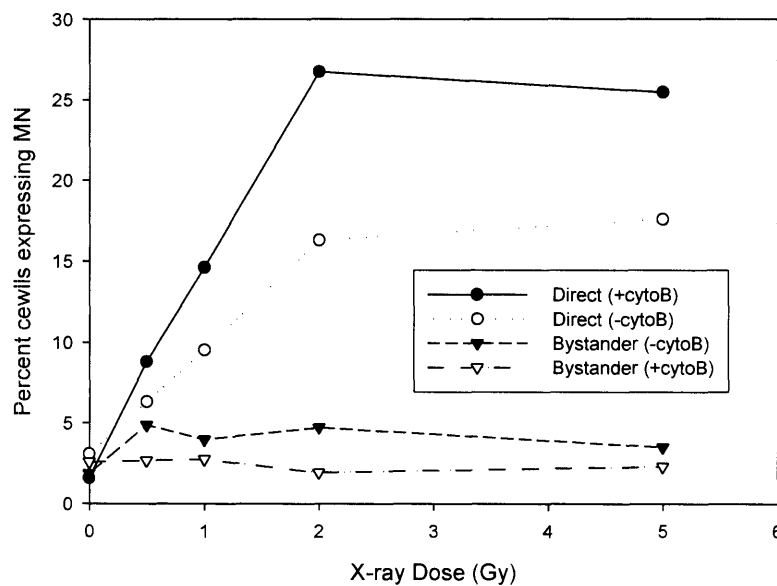
Figure 3-15: **Comparison of dose response curves for induction of MN in keratinocytes after x-rays with and without cytochalasin B.** Samples with cytochalasin B were fixed 72 h after irradiation. Samples without cytochalasin B were fixed at 24 h. Data shown are based on one experiment.

A dose response curve for MN bystander effect from keratinocytes to keratinocytes was obtained for x-rays and is shown in Figure 3-16. A linear curve is seen in MN response for directly irradiated cells up to 2 Gy, then a decline at 5 Gy. The bystander effect is also seen with a two-fold increase in MN expression in the keratinocyte bystander cells, 24 h after irradiation. The same assay was done with the Fe ion beam, but with time points of 24, 48 and 72 h after irradiation. Figure 3-17 shows the direct response of MN for the three time points in the keratinocytes after Fe ions. As seen, the largest MN expression for directly irradiated keratinocytes occurs after 48 hours. Table 3.1 shows the percent of MN expression in the bystander cells for the three time points after Fe irradiation. No conclusive bystander effect is seen in the keratinocytes in the form of MN from Fe beam irradiation.
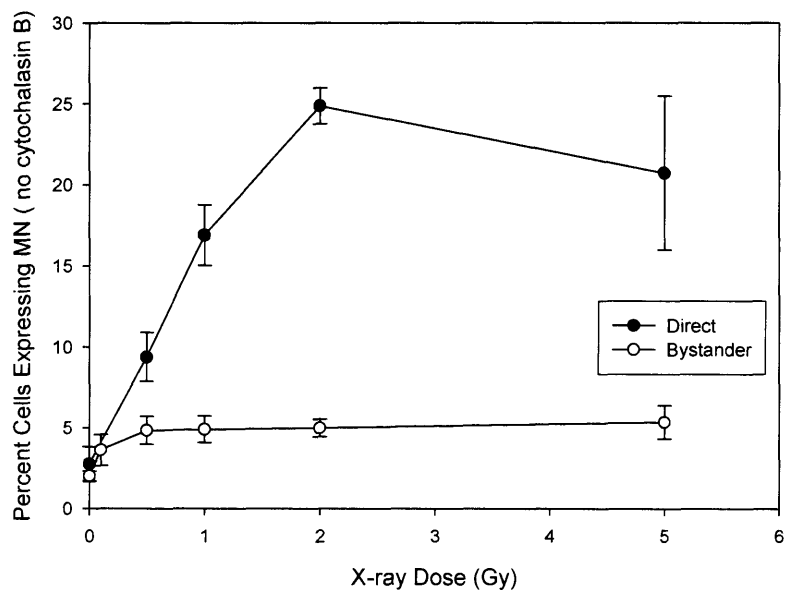
Figure 3-16: **Dose response for induction of micronuclei from directly irradiated and bystander keratinocyte cells 24 h after x-ray irradiation**. Data are the means of at least three experiments ± s.e.
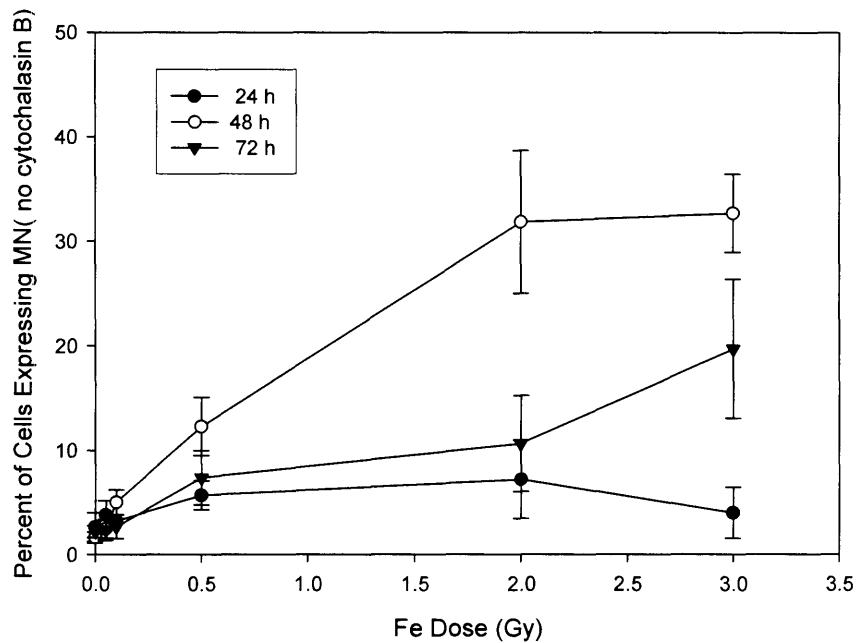
Figure 3-17: **Dose response for induction of micronuclei from directly irradiated keratinocyte cells 24, 48, and 72 h after Fe ion irradiation.** Data are the means of at least three experiments ± s.e.

(a) 24 hours			
Dose (Gy)	Experiment 1 Bystander % MN	Experiment 2 Bystander %MN	Experiment 3 Bystander %MN
0	1.6	1.4	
0.05	2.0	8.2	1.5
0.1	2.3	3.0	
0.5	1.7	3.6	1.9
2	1.3	5.1	0.77
3	0.99	4.1	1.2

(b) 48 hours			
Dose (Gy)	Experiment 1 Bystander % MN	Experiment 2 Bystander %MN	Experiment 3 Bystander %MN
0	1.8	3.1	0.9
0.05	2.4	3.1	1.3
0.1	2.6	4.5	0.53
0.5	1.7	4.7	0.55
2	3.1	5.3	1.5
3	1.3	4.8	1.1

(c) 72 hours			
Dose (Gy)	Experiment 1 Bystander % MN	Experiment 2 Bystander %MN	Experiment 3 Bystander %MN
0	0.93	3.0	0.56
0.05	0.93	2.6	1.1
0.1	2.9	4.2	
0.5	3.1	4.3	1.2
2	1.5	2.8	0.94
3	2.4	4.6	1.6

Table 3.1 **Dose response for induction of MN in keratinocyte bystander cells co-cultured with directly irradiated keratinocyte cells from Fe ion irradiation.** (a) 24 h; (b) 48 h; (c) 72 h after irradiation.

Once the bystander effect was seen via the induction of MN in keratinocytes after x-rays, the MN bystander effect from AGO1522 cells and keratinocytes was studied for both radiation types. Figure 3-18 shows the induction of MN in bystander keratinocytes co-cultured with directly irradiated AGO1522 cells, and Figure 3-19 shows the induction of MN in the bystander AGO1522 cells co-cultured with the directly irradiated keratinocytes for 24 hours after x-rays. The bystander keratinocytes show a two-fold increase in MN induction with a plateau reached by the 0.5 Gy x-ray dose to the AGO1522 cells. Similarly, the AGO1522 bystander cells show a two-fold increase in MN expression and the response plateaus roughly by 1 Gy x-rays to the keratinocytes.

AGO(D)Kera(I) - Kera(I) Graphed
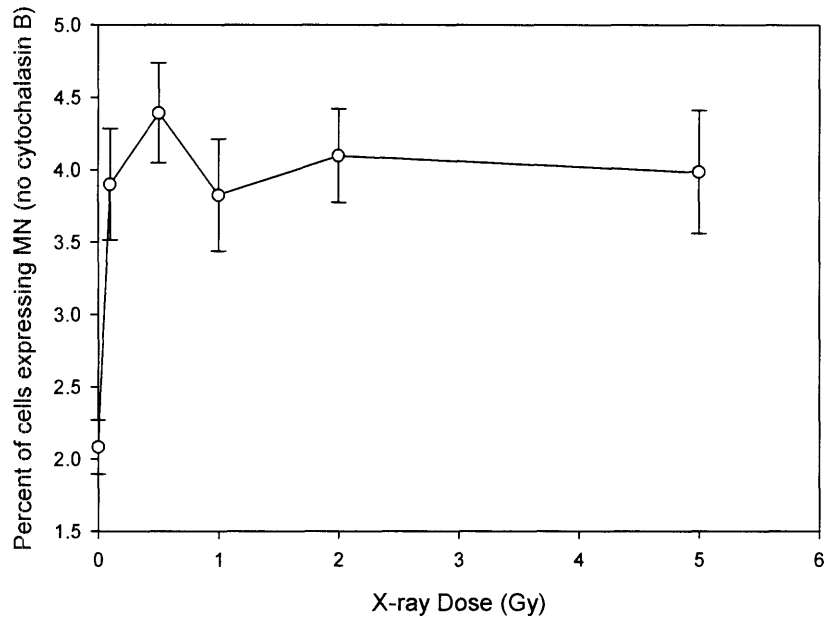
Figure 3-18: **Dose response for induction of MN in bystander keratinocyte cells co-cultured with directly irradiated AGO1522 cells for 24 h after x-rays.** Data are the means of at least three experiments ± s.e.
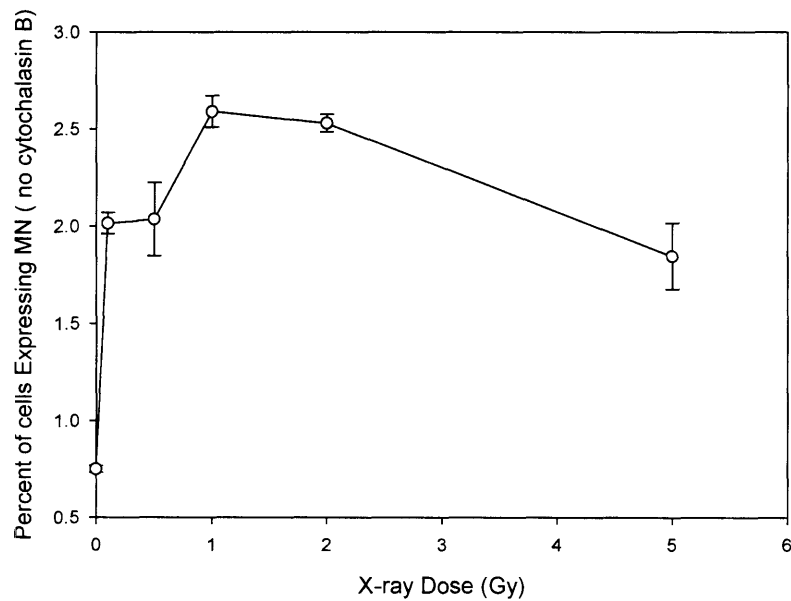
Figure 3-19: **Dose response for induction of MN in bystander AGO1522 cells co-cultured with directly irradiated keratinocyte cells for 24 h after x-rays.** Data are the means of at least three experiments ± s.e.

Data obtained for MN bystander induction from the co-cultures of the two cell lines

exposed to the Fe beam showed two major differences from the results with x-rays. First,

a bystander effect was seen from irradiated AGO1522 cells to keratinocyte bystander

cells, with a two-fold increase in expression, but no visible bystander effect was seen

from directly irradiated keratinocytes to AGO1522 cells at any of the four time points

tested, 5, 24, 40, and 50 h. Secondly, the bystander effect in keratinocytes was only seen

50 hours after irradiation of the AGO1522 cells with the Fe ion beam. Table 3.2

summarizes the above mentioned data.

(a) Keratinocyte (Bystander)	50 h	
Dose (Gy)	Experiment 1 % MN	Experiment 2 % MN
0	1.7	2.1
0.1	3.6	4.4
2	2.7	

(b) AGO1522 (Bystander)	50 h	
Dose (Gy)	Experiment 1 % MN	Experiment 2 % MN
0	0.92	1.4
0.1	0.97	1.7
2	1.1	1.9

Table 3.2 **Co-cultured bystander samples from Fe ion irradiation**. (a) Bystander
response in keratinocytes co-cultured with directly irradiated AGO1522 cells for 50 h
after Fe ion irradiation. (b) Bystander response in AGO1522 cells for co-cultured with
directly irradiated keratinocytes 50 h after Fe ion irradiation.

3.5 Chromatin Bridge Expression

Chromatin bridge expression was scored in irradiated and bystander keratinocytes for

both x-rays and Fe ion beam. Figure 3-20 shows an example of chromatin bridge

formation 48 h after 3 Gy of Fe ion beam in directly irradiated keratinocyte cells. The

chromatin bridges vary in length and width, and often are accompanied by micronuclei.

Also, as can be seen from the image, the cells appear to have distinct cytoplasms. Figure

3-21 shows the induction of chromatin bridges by x-rays in directly irradiated

keratinocytes, and Figure 3-22 shows the induction of chromatin bridges by Fe ions in

directly irradiated keratinocytes. Neither irradiation type showed a bystander effect via

chromatin bridge induction. Also, in the Fe ion data, it is seen that the chromatin bridge

expression is highest at 48 h, where the x-ray data are from cells fixed 24 h after

irradiation. The Fe ion data show that this radiation is more effective at inducing

chromatin bridges than x-rays.
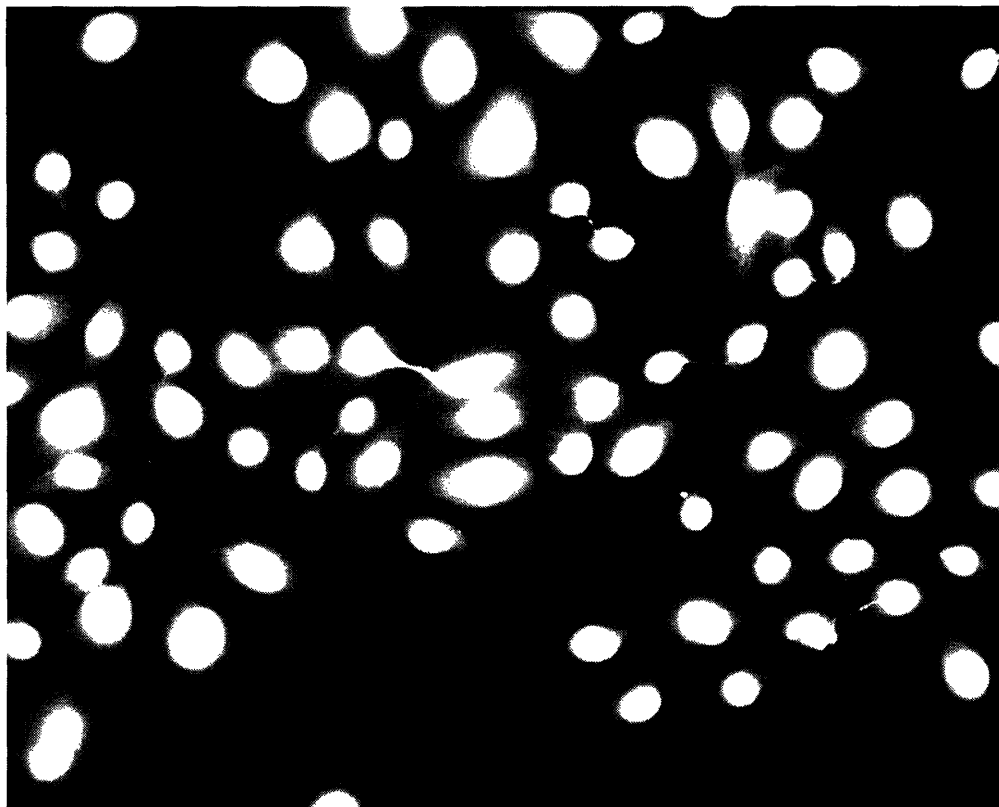
Figure 3-20: *In situ* **fluorescence detection of chromatin bridges in directly irradiated keratinocytes 48 h after 3 Gy of Fe ions.**
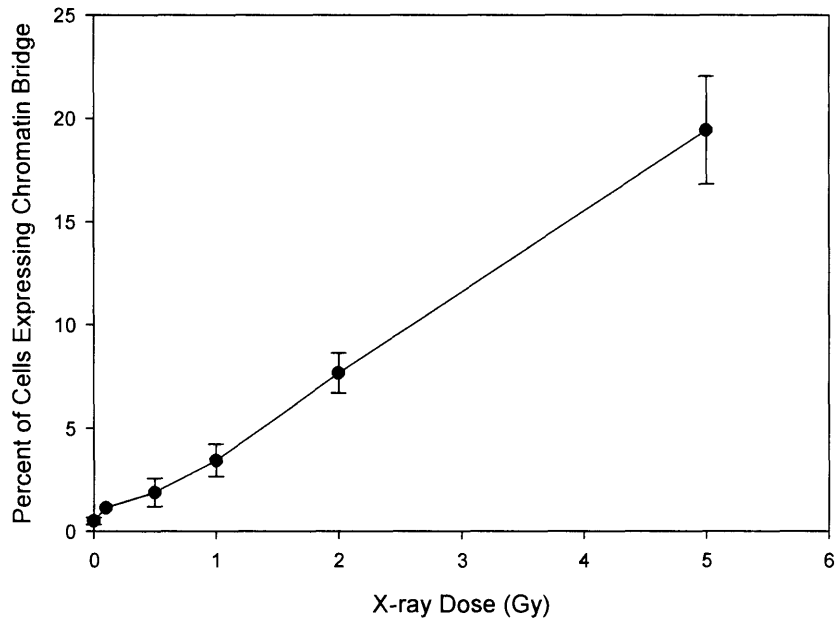
Figure 3-21: **Dose response for induction of chromatin bridges in directly irradiated keratinocyte cells 24 h after x-ray irradiation.** Data are the means of at least three experiments ± s.e.
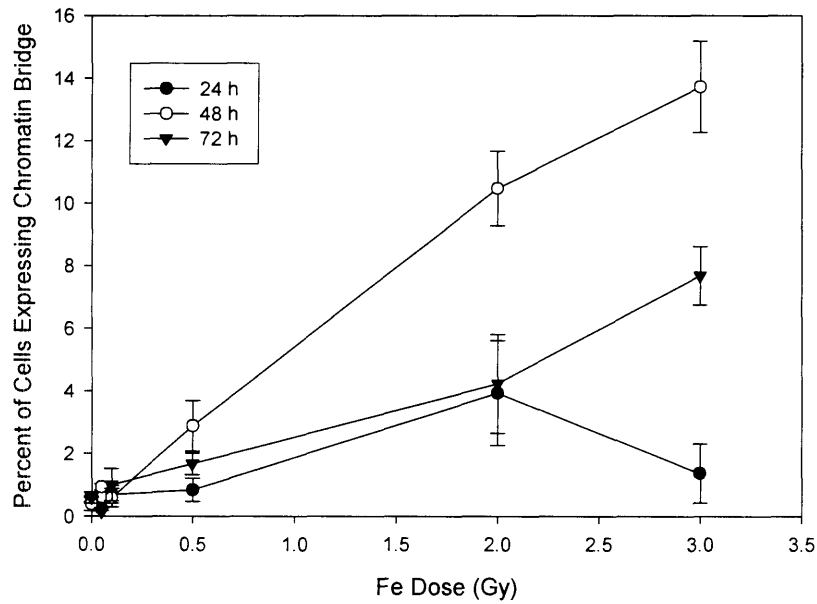
Figure 3-22: **Dose response for induction of chromatin bridges in directly irradiated keratinocyte cells 24, 48, and 72 h after Fe ion irradiation.** Data are the means of at least three experiments ± s.e.

Chapter 4

Discussion

4.1 Effects on Directly Irradiated Cells

A typical low LET survival curve has a prominent repair shoulder at the low doses before decreasing in survival in the exponential portion. A high LET curve shows no repair shoulder and is entirely exponential (Hall 2000). The curves obtained for keratinocytes after 250 kVp x-rays and 1000 MeV/nucleon Fe showed these trends. A repair shoulder is seen in the x-ray irradiation curve up until 2 Gy. The Fe ion beam is more effective at decreasing survival, where at 10% survival; an RBE is calculated at approximately 2.8.

The protein $p21^{wafl}$ is known to play a central role in DNA replication and cell cycle progression. It has been shown to be expressed downstream of p53, a tumor suppressor gene. In general, if $p21^{wafl}$ over expression is seen in cells with wild-type p53, then the cell has activated p53. By staining for $p21^{wafl}$, both $p21^{wafl}$ and p53 induction can be concluded (Fei and El-Deiry 2003). Looking at the $p21^{wafl}$ expression in directly irradiated keratinocyte cells, a sharp increase is seen by 1 Gy, and the response tends to plateau by 5 Gy at 24 hours after x-rays. From Fe ion irradiation however, $p21^{wafl}$ over expression as examined by immunofluorescence does not occur until 40-50 hours post irradiation. Yet, at 40-50 hours, the Fe ion beam is more effective at inducing $p21^{wafl}$

over expression than x-rays. Induction of p21^{wafl} in 25% of the cells gives an RBE of approximately 2.

It has been shown that upregulation of p21^{wafl} causes both G1 and or G2 arrests (Rigberg et al. 1999; Fei and El-Deiry 2003). From the x-ray data, it is seen that a slight G2 arrest is visible at 5 h as seen in figure 3-7, and is gone by 24 hours post irradiation in the keratinocytes. This suggests that after the G2 arrest, cells continue to divide and then the 24-hour expression of p21^{wafl} actually occurs in the daughter cells. In comparison, after iron irradiation, the cell cycle data show a strong G2 arrest at 5 hours and it lasts at least until 40-50 hours, Figure 3-13. Also, a decrease in S phase at 24 hours is noted and is still present at 50 hours. The data suggest that a strong G2 arrest is occurring until approximately 40 hours after irradiation, at which point cells start moving through the cycle and divide and that the daughter cells are then getting arrested in G1, shown by the persistent reduction of S phase. The arrest at G1 in the daughter cells is signaled by p21^{wafl} expression seen via immunofluorescence staining.

This strong G2 arrest has also been shown previously using wild type p53 glioblastoma cells by Tsuboi, *et al.* The group showed a strong G2 arrest in their cell type 12 h after 20 keV/μm, 40 keV/μm, 81 keV/μm, and 105 keV/μm carbon beam (Tsuboi et al. 1998). The group also reported a decrease in S phase, a sign of G1 arrest, but not as significant as the G2 block. They compared the response in their cells to cells treated using a ^{137}Cs gamma irradiation, and noted a G1 arrest 12 h after irradiation, but only in the p53 wild type. However, the group did not perform any flow cytometry analysis for longer time points. Another example of the cell cycle delays from heavy ions was published by Scholz *et al.* in synchronous cells (Scholz et al. 1994). The group showed a

strong delay in G2 for V79 Chinese hamster cells immediately after irradiation that persisted still at 48 h post irradiation via neon beam of LET 415 keV/μm, nickel ions of LET 2018 keV/μm, and titanium ions of LET 3020 keV/μm. Lastly Holgersson *et al.* showed a G2 arrest from 140 keV/μm nitrogen atoms in the human glioma cell lines M059J and M059K, where M059J is a cell line deficient in PKcs and has a decreased ability to repair DNA double strand breaks (Holgersson et al. 2005). The group showed a marked G2 arrest until 48 h after irradiation for both cell lines, but the arrest was still present in the deficient cell line up until 10 days after irradiation, where by 72 h the percentage of M059K in G2 decreased to control levels.

The cycle analysis provides not only a plausible explanation of the delays seen in p21^{wafl} expression in Fe ions compared to x-rays, it also explains the delay seen in production of micronuclei and chromatin bridges. Briefly, a micronucleus is a chromosome fragment that is not included with the rest of the nucleus at cell division. It has enough information to form its own nuclear membrane and looks like a mini nucleus, as seen in the image of Figure 3-14. Typical micronuclei analysis relies on the addition of cytochalasin B, an inhibitor of cell division by halting the formation of contractile microfilaments, and therefore stops cells in the binucleated form. The use of cytochalasin B ensures that when scoring a sample, a cell with a micronucleus in a binucleated cell is one that came from one parent. Initial experiments were done with cytochalasin B added for x-ray and Fe ion beam irradiation. Figure 3-15 shows one experiment with and without cytochalasin B addition for x-rays. It is seen that the addition of cytochalasin B decreased the percentage of cells with MN, but the trend was similar. This could be a toxicity issue of cytochalasin B in keratinocytes, since a low drug concentration, only 0.5

µg/ml was found to minimize toxicity to the cells. Both curves appear linear until 2 Gy, and fall off at 5 Gy. This response is again seen in the averaged MN production in directly irradiated cells without cytochalasin B in Figure 3-16. One plausible explanation for the decrease in production at 5 Gy is that by 5 Gy of x-rays less than 10% of the cells survive. Under the microscope, by 5 Gy most of the cells look smaller and there are far fewer cells attached, even though equal amounts of cells were plated initially for all doses. It therefore appears that at 5 Gy the cells are not dividing and are dying rapidly, perhaps due to permanent cell cycle arrests, so a decrease in MN will be seen. For x-rays, maximum production of MN was seen by 24 h, allowing a one-time division of the cells. In contrast, significant MN production after Fe ions was delayed as seen in Figure 3-17. Little to no direct expression is seen at 24 h, by 48 h it is maximum, and a reduction is seen by 72 h. The delay in MN production to 48 h after Fe irradiation is explained by the cell cycle analysis. Cells were at G2 arrest until 40-50 h after irradiation, at which point the decrease in G2 cells marked the transition of some cells from G2 into mitosis. The cells divided and therefore formation of MN can be seen. At 20% formation of MN, an RBE of 1.3 is seen when comparing the maximum effect at 24 h for x-ray to 48 h for Fe ions. A decrease in MN formation at 72 h after high doses can once more be explained with the fact that cells are most likely dying and floating off the slides, again seen by fewer cells on the slides giving the impression of cells not growing.

Another chromosomal damage that is seen in keratinocytes is chromatin bridges. Briefly, radiation can cause chromatin damage and perhaps cause it to break (Lengauer 2001). Normally a chromosome has telomere caps at its ends, but by breaking, it no longer has a telomere cap and the two broken ends can fuse together incorrectly and form

a chromosome with two centromeres. During cell division, this abnormal chromosome is pulled to both poles and in turn forms a long chromosome bridge between the two daughter cells, a chromatin bridge. Production of chromatin bridges was seen to have a fairly linear relationship with x-ray dose, Figure 3-21, for directly irradiated keratinocytes, with a maximum at 24 h. However, with Fe ions, the maximum chromatin bridge production did not occur until 48 h after irradiation, as seen in Figure 3-22. The response curve at 48 h is fairly linear with dose. Expression at 24 h and 72 h are almost identical, with exception of 5 Gy. The delay in appearance of bridges can once more be explained by radiation-induced cell cycle arrest. The keratinocytes were cell cycle arresting at G2 until 40 h and appeared to be moving through the cell cycle by 50 h. Therefore, division of the cells mostly occurred at around 40-50 and so formation of chromatin bridges would be highest then. Calculating an RBE at 10% chromatin bridge induction at maximum expression of 24 h for x-rays and 48 h for Fe ions, gives a value of 1.4. The value is stating that Fe ions are more effective at inducing chromatin bridges than x-rays.

Finally, it should be mentioned that apoptosis was checked for in keratinocytes both by fluorescent staining and by cell cycle analysis. Neither assay showed apoptosis in keratinocytes for either radiation type at the time points tested. However, visually on the slides it is seen that by the larger doses of both radiation types, the cells begin to look smaller and unhealthy, but no apoptotic bodies, a typical marker for apoptosis, is seen. This raises the question of what is the mode of death for the keratinocytes.

4.2 Effects on Bystander Cells

4.2.1 Keratinocyte to Keratinocyte

The experimental setup that was used in this work for the bystander effect has measured medium mediated effects. Therefore, whatever signal was released or stopped being released by the direct cells had to diffuse through almost a full centimeter of medium to induce an endpoint in the bystander cells. The protein $p21^{wafl}$ is frequently an endpoint that is used in bystander studies. The $p21^{wafl}$ bystander signal in keratinocytes to keratinocytes is shown in Figure 3-4 for x-rays, fixed 24 h after irradiation. It has the typical shape of a bystander curve, with a sharp increase in the bystander effect at the low doses, here at 0.1 Gy, and plateauing until 5 Gy. Other groups previously have showed this typical shape of the bystander curve. Yang *et al*. showed plateauing curves in AGO1522 bystander cells for $p21^{wafl}$, MN and γH_2AX and clonogenic endpoints (Yang et al. 2005). Mothersill and Seymour showed a plateauing bystander curve for clonogenic survival in human keratinocytes with a sharp decrease in survival at 0.5 Gy and plateauing until 10 Gy from gamma radiation of ^{60}Co (Mothersill and Seymour 1997). However, it is still unknown why the bystander effect increases rapidly at the low doses, and then plateaus out. A similar bystander curve is seen due to Fe ion beam in Figure 3-5. A two-fold increase in response is seen at 0.1 Gy and it also plateaus out by 2 Gy. The magnitude of the effect is the same for x-rays and Fe ions. However, for the Fe beam, the $p21^{wafl}$ bystander effect did not show up until 40-50 h after irradiation, mimicking the timing of the effect in the directly irradiated cells, whereas the bystander effect showed at 24 h for the x-rays. It is not clear why the bystander effect is also delayed from Fe ion irradiation. It hints at the idea that whatever the bystander signal might be, it is affected

by the G2 arrest of the directly irradiated cells. Perhaps for keratinocytes, the bystander signal is sent when the directly irradiated cells are at a certain phase of the cell cycle or once the cells divide, such that it is the daughter cells that are signaling.

Another common bystander endpoint is MN induction. As previously mentioned, typical MN assays call for addition of a cell division blocking agent, cytochalasin B. However it became apparent in this study that when cytochalasin B was added to x-ray irradiated cells, no bystander signal was seen at 24, 48, or 72 h (shown in Figure 3-15), but without cytochalasin B the bystander effect was seen at 24 h and at 48 h (not shown). Both time points showed equal bystander response and so 24 h was chosen as the time of assay. Figure 3-16 shows the average bystander response from at least three experiments. Again, the sharp increase at low doses is seen, then a plateauing at the higher doses. The data suggest that cytochalasin B somehow interferes with the bystander signal for the MN endpoint. Experiments with Fe beam irradiation were also performed with and without the addition of cytochalasin B. However, from the Fe beam, there is not an appearance of the MN bystander signal, as shown in Table 3.1 for 24, 48, or 72 h without cytochalasin B, and no bystander signal was seen with the addition of cytochalasin B (not shown). This suggests that the signal that induces a p21^{waf1} bystander effect is different from that for a MN bystander effect from Fe ion beam. Also, the signals from cells after x-rays for MN bystander must be different than for Fe ions, given the absence of a bystander effect for Fe ions. It should be noted that no chromatin bridge bystander effect was seen with either x-rays or Fe ions.

4.2.2 AGO1522 cells to Keratinocytes

A long-term goal of the bystander studies is to assess the bystander effects in tissues from x-rays and heavy ions. Keratinocytes and the human fibroblast AGO1522 cells are both common cells used in tissue models. To compare with the bystander effect from keratinocyte to keratinocyte cells, the same endpoints were investigated using mixed cell co-cultures. Figure 3-6 shows the p21^{wafl} bystander response of keratinocytes after 24 h of co-culture with AGO1522 cells that have exposed to x-rays. Once again the sharp increase in the bystander effect is seen at the low doses and the response plateaus out to 5 Gy. The effect shows an approximate 2.5 fold increase in p21^{wafl} expression. Similarly Figure 3-18 shows the MN bystander expression in keratinocytes after 24 h of co-culture with AGO1522 cells exposed to x-rays. Again the typical curve is seen and a two-fold increase is apparent. Table 3.2 (a) compares the MN bystander data for keratinocytes co-cultured with AGO1522 cells treated with Fe ions. The data, although preliminary, show a possibility of a bystander effect with the keratinocytes at 50 h after Fe irradiation to the fibroblasts, but no potential bystander signal was seen at 5, 24, or 40 h after Fe ion irradiation. This indicates a difference between the x-ray data and the Fe ion data. A clear MN bystander effect at 24 h was seen in keratinocytes exposed to fibroblasts treated with x-rays, where the Fe ion data shows only a potential bystander effect and only at 50 h. Again, timing of the signal appears important even in the mixed cell lines after the Fe ion beam exposure.

4.2.3 Keratinocyte to AGO1522 cells

A bystander signal from directly irradiated keratinocytes co-cultured with AGO1522 cells was also investigated. Figure 3-19 shows the MN bystander response at 24 h in

AGO1522 cells that had been co-cultured with directly irradiated keratinocytes treated with x-rays. A typical shape of the curve is seen with a 2-fold bystander effect signal. In comparison, no bystander effect at 5, 24, 40, or 50 h was seen in AGO1522 cells co-cultured with keratinocytes treated with Fe as shown in Table 3.2 (b). This mimics the signaling responses that were seen in keratinocytes co-cultured with keratinocytes treated with either x-rays or Fe ions. Briefly, keratinocytes co-cultured with keratinocytes that were treated with x-rays had a 24 h MN bystander response but no MN bystander response from Fe ion exposure. The fact that AGO1522 cells received at 24 h bystander signal from keratinocytes treated with x-rays but not from Fe ion exposures at any of the time points studied makes it appear that keratinocytes are signaling a MN bystander effect from x-rays but not from Fe ions. Also this implies that the AGO1522 cells are reacting to the same signal that is emitted from keratinocytes co-cultured with keratinocytes for the MN bystander expression.

Chapter 5

Conclusion

Differences between 250 kVp x-rays and 1000 MeV/nucleon Fe ion beam in both directly irradiated and bystander keratinocytes were very apparent. Iron was more effective at causing cell death than the x-rays. For directly irradiated cells, the iron was more effective at inducing damage with endpoints of p21^{waf1} expression, MN induction, and chromatin bridge induction. Also, cell cycle differences were apparent with only a slight G2 arrest from x-rays at 5 h but a pronounced G2 arrest still present at 40-50 h, followed by an S phase reduction from Fe ions. From x-rays, keratinocytes showed maximal expression of p21^{waf1} protein, MN, and chromatin bridges at 24 h after irradiation. Due to the cell cycle arrests, keratinocytes had a delay of 40-50 h for MN expression, chromatin bridges, and p21^{waf1} expression by immunofluorescence in directly irradiated cells from Fe ions. No induction of apoptosis at the tested time points was seen from either beam.

The keratinocytes co-cultured with keratinocytes showed a bystander effect with a two-fold increase in p21^{waf1} induction 24 h after irradiation with x-rays. Similarly, a p21^{waf1} bystander effect was seen in the keratinocytes from Fe beam irradiation, but only 40-50 h after irradiation. It is unclear why the bystander response is delayed. Perhaps the cell cycle delays in the directly irradiated cells somehow delay the bystander signal or the bystander signal is emitted only during a certain phase of the cell cycle. For MN

induction, the addition of the cytokinesis blocking drug cytochalasin B inhibited the bystander signal from both x-rays and Fe ions. When the drug was not added, a 2-fold MN bystander was seen with x-rays 24 h after irradiation but no MN bystander was seen for the Fe ions at any of the time points studied after irradiation. This gives the impression that the bystander signal is different for p21^{wafl} induction and MN since p21^{wafl} induction was seen with both beams. Also, the MN bystander signal is somehow not released from cells irradiated with Fe ions but is released from keratinocyte cells that are directly irradiated with x-rays. This also brings up the issue of whether it is dead or alive cells that release the bystander signal. From Fe irradiation, the number of cells that survive is far fewer than cells after x-ray irradiation. Perhaps the possibility of fewer live cells has an effect on the bystander effect signal for each of the endpoints. Or another possibility is that the bystander signals from cells treated with Fe ions and x-rays are different for the various endpoints.

AGO1522 cells signaled a bystander response in keratinocytes via p21^{wafl} induction and MN production 24 h after x-rays. Preliminary data show a MN bystander response in keratinocytes from AGO1522 cells only 50 h after Fe irradiation. It is unclear why the bystander response in the keratinocytes is also delayed. A MN response was seen in bystander AGO1522 cells co-cultured with directly irradiated keratinocytes 24 h after x-rays but no bystander response was seen at any of the time points studied with Fe ions. Again, this hints that the keratinocytes are unable to signal a MN bystander response after Fe ion irradiation. Also, this suggests that the AGO1522 cells are responding to the same bystander signal that is emitted from the irradiated keratinocytes to unirradiated keratinocytes.

Although the mechanisms of the bystander signal in the keratinocytes are still unknown, several novel results have been described. The bystander effect has been shown in co-cultured samples from cells treated with x-rays and Fe ions. Several delays and possible effects of the cell cycle from Fe ion irradiation on the bystander signal have been put forth. Future work will continue to develop the full picture and clarify the bystander effect from heavy ions such as Fe ion beam.

5.1 Future Work

In addition to using a 1 GeV/nucleon Fe beam, further studies with a medium LET ion such as carbon and low LET ion such as protons should be performed to look at the correlations between LET and the bystander effect. More importantly, data presented here are of a one time irradiation of a single ion and at times of a high dose, whereas in space dose is continuous, a mixture of types of LET, and of low particle fluence. Further studies are needed with the keratinocytes using a mixed beam of low particle fluence in order to more accurately mimic the radiation environment in space. However, at such low fluences, cells can be irradiated by either the heavy ion directly or with a delta ray. In a study done by Brooks et al. in rats with ^{56}Fe particles (1 GeV/nucleon), for every cell traversed by a primary iron particle, it was estimated that 32 cells were hit by delta rays (Brooks et al. 2001). Thus, detection methods must be developed that can determine which cells in a population were exposed to the heavy ion, to the delta rays, or were not irradiated. In these experimental conditions, the unirradiated cells are then the bystander cells.

Bibliography

Azzam, E. I., S. M. de Toledo, et al. (1998). "Intercellular communication is involved in the bystander regulation of gene expression in human cells exposed to very low fluences of alpha particles." Radiat Res 150(5): 497-504.

Azzam, E. I., S. M. de Toledo, et al. (2001). "Direct evidence for the participation of gap junction-mediated intercellular communication in the transmission of damage signals from alpha -particle irradiated to nonirradiated cells." Proc Natl Acad Sci U S A 98(2): 473-8.

Ballarini, F., M. Biaggi, et al. (2002). "Cellular communication and bystander effects: a critical review for modelling low-dose radiation action." Mutat Res 501(1-2): 1-12.

BEIRVII (2005). Health Risks from Exposure to Low Levels of Ionizing Radiation. Committee to Assess Health Risks from Exposure to Low Levels of Ionizing Radiation, National Academy of Sciences.

Blakely, E. A. (2000). "Biological effects of cosmic radiation: deterministic and stochastic." Health Phys 79(5): 495-506.

Brooks, A., S. Bao, et al. (2001). "Relative effectiveness of HZE iron-56 particles for the induction of cytogenetic damage in vivo." Radiat Res 155(2): 353-9.

Chatterjee, A. and H. J. Schaefer (1976). "Microdosimetric structure of heavy ion tracks in tissue." Radiat Environ Biophys 13(3): 215-27.

Concin, N., M. Stimpfl, et al. (2003). "Role of p53 in G2/M cell cycle arrest and apoptosis in response to gamma-irradiation in ovarian carcinoma cell lines." Int J Oncol 22(1): 51-7.

Cucinotta, F. (2000). "Once we know all the radiobiology we need to know, how can we use it to predict space radiation risks and achieve fame and fortune?" 11th Annual NASA Space Radiation Health Investigators' Workshop.

Curtis, S. B. and J. R. Letaw (1989). "Galactic cosmic rays and cell-hit frequencies outside the magnetosphere." Adv Space Res 9(10): 293-8.

Dickson, M. A., W. C. Hahn, et al. (2000). "Human keratinocytes that express hTERT
and also bypass a p16(INK4a)-enforced mechanism that limits life span become
immortal yet retain normal growth and differentiation characteristics." Mol Cell
Biol 20(4): 1436-47.

Fei, P. and W. S. El-Deiry (2003). "P53 and radiation responses." Oncogene 22(37):
5774-83.

Fenech, M. and A. A. Morley (1986). "Cytokinesis-block micronucleus method in human
lymphocytes: effect of in vivo ageing and low dose X-irradiation." Mutat Res
161(2): 193-8.

Gisselsson, D., L. Pettersson, et al. (2000). "Chromosomal breakage-fusion-bridge events
cause genetic intratumor heterogeneity." Proc Natl Acad Sci U S A 97(10): 5357-
62.

Goodhead, D. T. (1995). "Molecular and cell models of biological effects of heavy ion
radiation." Radiat Environ Biophys 34(2): 67-72.

Hall, E. (2000). Radiobiology for the Radiobiologist. New York, Lippincott Williams &
Wilkins.

Holgersson, A., T. Heiden, et al. (2005). "Different G2/M accumulation in M059J and
M059K cells after exposure to DNA double-strand break-inducing agents." Int J
Radiat Oncol Biol Phys 61(3): 915-21.

Knoll, G. (1999). Radiation Detection and Measurement. New York, John Wiley & Sons.

Lengauer, C. (2001). "How do tumors make ends meet?" Proc Natl Acad Sci U S A
98(22): 12331-3.

Lyng, F. M., C. B. Seymour, et al. (2000). "Production of a signal by irradiated cells
which leads to a response in unirradiated cells characteristic of initiation of
apoptosis." Br J Cancer 83(9): 1223-30.

Masumura, K., K. Kuniya, et al. (2002). "Heavy-ion-induced mutations in the gpt delta
transgenic mouse: comparison of mutation spectra induced by heavy-ion, X-ray,
and gamma-ray radiation." Environ Mol Mutagen 40(3): 207-15.

Mothersill, C. and C. Seymour (1997). "Medium from irradiated human epithelial cells
but not human fibroblasts reduces the clonogenic survival of unirradiated cells."
Int J Radiat Biol 71(4): 421-7.

Mothersill, C. and C. Seymour (2001). "Radiation-induced bystander effects: past history
and future directions." Radiat Res 155(6): 759-67.

Mothersill, C. and C. B. Seymour (1998). "Cell-cell contact during gamma irradiation is not required to induce a bystander effect in normal human keratinocytes: evidence for release during irradiation of a signal controlling survival into the medium." Radiat Res **149**(3): 256-62.

Nagasawa, H. and J. B. Little (1992). "Induction of sister chromatid exchanges by extremely low doses of alpha-particles." Cancer Res **52**(22): 6394-6.

Nagasawa, H. and J. B. Little (1999). "Unexpected sensitivity to the induction of mutations by very low doses of alpha-particle radiation: evidence for a bystander effect." Radiat Res **152**(5): 552-7.

Nilsson, J. R., T. R. Ricketts, et al. (1973). "Effects of cytochalasin B on cell division and vacuole formation in Tetrahymena pyriformis GL." Exp Cell Res **79**(2): 456-9.

Rigberg, D. A., T. A. Blinman, et al. (1999). "Antisense blockade of p21/WAF1 decreases radiation-induced G2 arrest in esophageal squamous cell carcinoma." J Surg Res **81**(1): 6-10.

Ritter, S., W. Kraft-Weyrather, et al. (1992). "Induction of chromosome aberrations in mammalian cells after heavy ion exposure." Adv Space Res **12**(2-3): 119-25.

Scholz, M., W. Kraft-Weyrather, et al. (1994). "Cell cycle delays induced by heavy ion irradiation of synchronous mammalian cells." Int J Radiat Biol **66**(1): 59-75.

Shao, C., M. Folkard, et al. (2004). "Targeted cytoplasmic irradiation induces bystander responses." Proc Natl Acad Sci U S A **101**(37): 13495-500.

Shao, C., Y. Furusawa, et al. (2003). "Role of gap junctional intercellular communication in radiation-induced bystander effects in human fibroblasts." Radiat Res **160**(3): 318-23.

Shao, C., Y. Furusawa, et al. (2002). "Nitric oxide-mediated bystander effect induced by heavy-ions in human salivary gland tumour cells." Int J Radiat Biol **78**(9): 837-44.

Shao, C., Y. Furusawa, et al. (2003). "Bystander effect induced by counted high-LET particles in confluent human fibroblasts: a mechanistic study." Faseb J **17**(11): 1422-7.

Shukitt-Hale, B., G. Casadesus, et al. (2000). "Spatial learning and memory deficits induced by exposure to iron-56-particle radiation." Radiat Res **154**(1): 28-33.

Smith, L. E., S. Nagar, et al. (2003). "Radiation-induced genomic instability: radiation quality and dose response." Health Phys **85**(1): 23-9.

Sutherland, B. M., P. V. Bennett, et al. (2001). "Clustered DNA damages induced by high and low LET radiation, including heavy ions." <u>Phys Med</u> **17 Suppl 1**: 202-4.

Thomas, P., K. Umegaki, et al. (2003). "Nucleoplasmic bridges are a sensitive measure of chromosome rearrangement in the cytokinesis-block micronucleus assay." <u>Mutagenesis</u> **18**(2): 187-94.

Tsuboi, K., Y. Tsuchida, et al. (1998). "Cytotoxic effect of accelerated carbon beams on glioblastoma cell lines with p53 mutation: clonogenic survival and cell-cycle analysis." <u>Int J Radiat Biol</u> **74**(1): 71-9.

Turner, J. (1995). <u>Atoms, Radiation and Radiation Protection</u>. New York, John Wiley & Sons.

Wilson, J. W. (2000). "Overview of radiation environments and human exposures." <u>Health Phys</u> **79**(5): 470-94.

Worgul, B. V., C. Medvedovsky, et al. (1989). "Accelerated heavy ions and the lens. IV. Biomicroscopic and cytopathological analyses of the lenses of mice irradiated with 600 MeV/amu 56Fe ions." <u>Radiat Res</u> **120**(2): 280-93.

Wu, L. J., G. Randers-Pehrson, et al. (1999). "Targeted cytoplasmic irradiation with alpha particles induces mutations in mammalian cells." <u>Proc Natl Acad Sci U S A</u> **96**(9): 4959-64.

Yang, H., N. Asaad, et al. (2005). "Medium-mediated intercellular communication is involved in bystander responses of X-ray-irradiated normal human fibroblasts." <u>Oncogene</u> **24**(12): 2096-103.